RUVBL1/2 Blockade Targets YTHDF1 Activity to Suppress m^{6}A-Dependent Oncogenic Translation and Colorectal Tumorigenesis

Danyu Chen[1], Fenfen Ji[1], Qiming Zhou[1], Henley Cheung[1], Yasi Pan[1], Harry C.-H. Lau[1], Cong Liang[1], Zhenjie Yang[1], Pingmei Huang[1], Qinyao Wei[1], Alvin H.-K. Cheung[2], Wei Kang[2], Huarong Chen[3], Jun Yu[1], and Chi Chun Wong[1]

ABSTRACT

The N^6-methyladenosine (m^{6}A) RNA-binding protein YTHDF1 is frequently overexpressed in colorectal cancer and drives chemotherapeutic resistance. To systematically identify druggable targets in colorectal cancer with high expression of YTHDF1, this study used a CRISPR/Cas9 screening strategy that revealed RUVBL1 and RUVBL2 as putative targets. RUVBL1/2 were overexpressed in primary colorectal cancer samples and represented independent predictors of poor patient prognosis. Functionally, loss of RUVBL1/2 preferentially impaired the growth of YTHDF1-high colorectal cancer cells, patient-derived primary colorectal cancer organoids, and subcutaneous xenografts. Mechanistically, YTHFD1 and RUVBL1/2 formed a positive feedforward circuit to accelerate oncogenic translation. YTHDF1 bound to m^{6}A-modified RUVBL1/2 mRNA to promote translation initiation and protein expression. Coimmunoprecipitation and mass spectrometry identified that RUVBL1/2 reciprocally interacted with YTHDF1 at 40S translation initiation complexes. Consequently, RUVBL1/2 depletion stalled YTHDF1-driven oncogenic translation and nascent protein biosynthesis, leading to proliferative arrest and apoptosis. Ribosome sequencing revealed that RUVBL1/2 loss impaired the activation of MAPK, RAS, and PI3K-AKT signaling induced by YTHDF1. Finally, the blockade of RUVBL1/2 by the pharmacological inhibitor CB6644 or vesicle-like nanoparticle-encapsulated siRNAs preferentially arrested the growth of YTHDF1-expressing colorectal cancer *in vitro* and *in vivo*. Our findings show that RUVBL1/2 are potential prognostic markers and druggable targets that regulate protein translation in YTHDF1-high colorectal cancer.

Significance: RUVBL1/2 inhibition is a therapeutic strategy to abrogate YTHDF1-driven oncogenic translation and overcome m^{6}A dysregulation in colorectal cancer.

Introduction

Colorectal cancer is one of the most common cancers worldwide (1). Despite great progress in diagnosis and therapy, patients with colorectal cancer frequently suffer from tumor metastasis and recurrence, leading to poor survival. Colorectal cancer is a multifactorial disease involving interplay of genetic, epigenetic, and environmental factors. Recent studies have also shed light on the crucial role of epitranscriptomics, chemical modifications in RNA, on colorectal tumorigenesis (2, 3). In particular, N^6-methyladenosine (m^{6}A) RNA modification, the most abundant modification in mRNA, has been associated with the development of multiple cancers (4). M^{6}A modification regulates mRNA splicing, degradation and translation, and their levels are tightly controlled by m^{6}A "writers" (METTL3/METTL14/WTAP) and "erasers" (ALKBH5/FTO; refs. 5, 6). The fate of m^{6}A-modified mRNAs is determined by their interaction with m^{6}A readers, including members of the YTH domain family (YTHDF/YTHDC; ref. 6) and insulin-like growth factor 2 mRNA-binding protein family (IGF2BP; ref. 7). Deregulation of m^{6}A regulators has multifaceted effects in tumor initiation, progression, metastasis, and modulation of tumor immune microenvironment (6, 8, 9).

YTHDF1 is one of the most studied m^{6}A readers, and studies, including ours, have demonstrated that YTHDF1 is overexpressed in many cancers such as colorectal cancer (6, 10). YTHDF1 is the most highly upregulated m^{6}A regulator in colorectal cancer, and YTHDF1 copy number gain is found in as much as 70% of colorectal cancer patients (6). Functional investigation by us highlights the role(s) of YTHDF1 in tumor metastasis and the modulation of antitumor immunity (6, 9, 10). In light of the important roles of YTHDF1 in colorectal cancer, it represents an attractive drug target for intervention. Nevertheless, there is no pharmacological agents that effectively suppress function of YTHDF1 in coloretal cancer. Hence, there is an urgent need to develop drugs targeting YTHDF1-m^{6}A-driven colorectal tumorigenesis.

The application of CRISPR-Cas9 pooled gene libraries coupled with high throughput sequencing has emerged as a powerful tool for the systematic identification of essential or fitness genes governing cell proliferation and survival (11–13) in a mixed cell

[1]Institute of Digestive Disease and Department of Medicine and Therapeutics, State Key Laboratory of Digestive Disease, Li Ka Shing Institute of Health Sciences, The Chinese University of Hong Kong, Hong Kong SAR, China. [2]Department of Anatomical and Cellular Pathology, The Chinese University of Hong Kong, Hong Kong SAR, China. [3]Department of Anaesthesia and Intensive Care, The Chinese University of Hong Kong, Hong Kong SAR, China.

Corresponding Authors: Chi Chun Wong, Department of Medicine and Therapeutics, Prince of Wales Hospital, The Chinese University of Hong Kong, Hong Kong SAR, China. E-mail: chichun.wong@cuhk.edu.hk; and Jun Yu, junyu@cuhk.edu.hk

Cancer Res 2024;84:2856–72

doi: 10.1158/0008-5472.CAN-23-2081

population. To systematically screen druggable genes in an unbiased manner, we constructed an inhouse Epi-Drug single-guide RNA (sgRNA) library comprising all druggable genes targeted by drugs approved by the Food and Drug Administration (Drugbank v.5.0) together with epigenetic regulators (~1,000 genes; refs. 14, 15). Here, we utilized this Epi-Drug library to identify gene targets that are preferentially effective in YTHDF1-overexpressed colorectal cancer.

To systematically screen for druggable targets in context of high YTHDF1 expression in colorectal cancer in this study, we performed Epi-Drug sgRNA library screening in colorectal cancer with YTHDF1 overexpression or knockout. Among genes that were preferentially effective in YTHDF1-high cells compared with YTHDF1-null cells, we identified RuvB like AAA ATPase 1/2 (RUVBL1/2) as unique, top-ranking candidates that preferentially inhibited YTHDF1-high colorectal cancer cells. RUVBL1/2 are respectively located on chromosomes 3q21.3 and 19q13.33, and they encode components of a protein complex with DNA-dependent ATPase activity. In addition, they are a scaffold protein for many cellular processes (16). Nevertheless, their function in translation is unclear. We validated that RUVBL1/2 loss preferentially suppressed YTHDF1-high colorectal cancer *in vitro* and *in vivo*. Moreover, we demonstrated that YTHDF1 and RUVBL1/2 function in a positive feedforward cycle that promotes protein translation and cancer signaling. Finally, pharmacological inhibitors or vesicle-like PLGA-based siRNA nanoparticles (VNPs-siRNA) targeting RUVBL1/2 inhibited the growth of YTHDF1-overexpressing colorectal cancer cells and xenografts. Together, our work indicates RUVBL1/2 as novel drug targets for the treatment of colorectal cancer with high YTHDF1 expression.

Materials and Methods

Cell lines

DLD1 (RRID: CVCL_0248), HCT116 (RRID: CVCL_0291), LOVO (RRID: CVCL_0399), SW480 (RRID: CVCL_0546), SW1116 (RRID: CVCL_0544), and HT29 (RRID: CVCL_0320) cells were all acquired from the ATCC. NCM460 cells were obtained from INCELL. All cell lines were authenticated by STR assay in March–April 2024 at the latest. All experiments were performed with cells that underwent 10 passages of thawing. All cells were cultured in DMEM (Gibco, 11965118) supplemented with 10% (v/v) fetal bovine serum (Gibco, 16140071) and antibiotic-antimycotic (Gibco, 15240112) at 37°C and 5% CO_2.

Human colorectal cancer cohorts

Four colorectal cancer patient cohorts were included in this study. Cohort 1 composed of 150 paired adjacent normal and colorectal cancer tissues collected from the Beijing University Cancer Hospital. Specimens were snap frozen in liquid nitrogen and then at −80°C until RNA extraction. Cohort 2 is the colorectal adenocarcinoma The Cancer Genome Atlas (TCGA) data (PanCancer Atlas) acquired from Xenabrowser (https://xenabrowser.net/), and it consists of 51 adjacent normal and 635 colorectal cancer tissues. Cohort 3 consists of protein samples from paired adjacent normal and colorectal cancer tissues collected at the Prince of Wales Hospital, Hong Kong. Cohort 4 from Beijing University Cancer Hospital included 184 colorectal cancer cases. Paraffinized tumor blocks of this cohort were used to establish the tissue microarrays (TMA). The clinicopathological features of colorectal cancer cohorts were provided in Supplementary Tables S1 and S2. Written informed consent was obtained from all patients. The study was conducted in accordance with the Declaration of Helsinki and was approved by human ethics committee of the Chinese University of Hong Kong (Ref. No. 2019.425).

RT-qPCR

Total RNA was isolated with TRIzol reagent and converted into cDNA using PrimeScript RT Reagent Kit (Takara, RR037B). Quantitative PCR (qPCR) was performed with One-Step TB Green PrimeScript RT-PCR Kit II (Takara; RR086B). Assays were conducted in triplicates in the ViiA7 Real-Time PCR System (Thermo Fisher Scientific) in a 96- or 386-well plate format. *ACTB* was used as an internal control. Relative expression was examined using $2^{-\Delta\Delta CT}$ method. Primers used in this study are shown in Supplementary Table S3.

CRISPR library screening

Pooled Epi-Drug sgRNA library was constructed as described (14, 15). DLD1 (RRID: CVCL_0248) and HCT116 (RRID: CVCL_0291) cells were first stably transfection with Cas9-FLAG and then transduced with pooled sgRNA library lentiviral supernatant (MOI < 0.3), with minimum representation of 500 per sgRNA. Two day posttransduction, cells were selected with puromycin for 6 days and then further transfected vector/YTHDF1-OE and shControl/shYTHDF1 lentivirus. Cells were then cultured in DMEM without puromycin for 14 days. Day 0 and day 14 samples were collected (approximately 20 million cells per sample) for DNA extraction and next-generation sequencing (IGEbio). For data analysis, NGS data were aligned to pooled library sgRNA sequences using Bowtie version 1.2.2 (RRID: SCR_005476). The reads count for every sgRNA was then computed by a custom Python script. Next, we utilized MAGeCK to estimate depleted or enriched genes at each time point (17).

YTHDF1 overexpression and knockdown in colorectal cancer cells

Wildtype YTHDF1 or mutant YTHDF1 (K395A, Y397A) was cloned into pLentiCMV-Hygro. shRNAs were cloned into pLKO.1-puro vector (RRID: Addgene_139470). The vectors were cotransfected into HEK293T (RRID: CVCL_0063) with packaging vectors pMDLg/pRRE (RRID: Addgene, 12251), pRSV-REV (RRID: Addgene, 12253), and pMD2.G (RRID: Addgene: 12259). Lentivirus containing medium was harvested 48 to 72 hours posttransfection and passed through a 0.22 μm filter. Transduction was performed with the addition of polybrene (4–8 μg/mL) for 24 hours. Overexpression and knockdown cells were selected with Hygromycin at 50 μg/mL and 1 μg/mL puromycin, respectively, for 1 to 2 weeks to obtain stable cell lines.

CRISPR/Cas9 knockout

To knockout RUVBL1/2, we designed single-guide RNAs (sgRNA) using the CRISPR tool (http://crispr.mit.edu) and cloned into LentiCRISRPv2 vector (Addgene, #52961); they were co-transfected with packaging vectors to HEK293T cells to generate lentivirus. To generate the knockout clones, DLD1 or HCT116 cells were transduced with lentivirus, and after 48 hours, cells were selected with puromycin at 1 μg/mL for 1 to 2 weeks to obtain stable cells.

RUVBL1/2 overexpression

For overexpression of wildtype and ATPase-dead mutant RUVBL1/2, we constructed pCDH-CMV-RUVBL1, pCDH-CMV-RUVBL1-E303Q, pCDH-CMV- RUVBL2 and pCDH-CMV-RUVBL2-E266Q plasmids and packaged into lentivirus as mentioned above. Transduction was performed with the addition of polybrene (4–8 μg/mL) for 24 hours. Overexpression cells were selected with Blasticidin at 5 μg/mL, for 1 to 2 weeks to obtain stable cell lines.

MTT assay

For cell viability assay, we used 3-(4,5-dimethylthiazol-2-yl)-2,5-diphenyltetrazolium (MTT, 5 mg/mL; Invitrogen). One thousand cells per well were seeded onto a 96-well plate. Cell viability was determined by incubation with MTT for 4 hours, followed by the addition of DMSO and measurement of absorbance at 570 nm. All experiments were conducted with 5 to 10 replicates per group.

Colony formation assay

For colony formation assay, 1,000 cells per well were seeded onto a six-well plate. Culture medium was changed every 3 days. After 10 to 14 days, colonies were fixed by ice-cold methanol and stained by 0.1% crystal violet. Cell colonies were measured by ImageJ (RRID: SCR_003070). All experiments were conducted in triplicates.

Apoptosis and cell cycle assays

Apoptosis was evaluated by FITC Annexin V Apoptosis Detection Kit (BD Biosciences) according to manufacturer's instructions. For cell cycle assay, cells were collected, fixed in 70% ethanol at −20°C overnight, and stained with propidium iodide/RNase (50 μg/mL; BD Biosciences) at room temperature for 15 minutes in dark. All stained cells were analyzed by flow cytometer (BD FACSCelesta Flow Cytometer, BD Biosciences). Data were analyzed by FlowJo (version 10.4; RRID:SCR_008520).

Immunofluorescence

Cells grown on glass coverslips were fixed with ice-cold 4% paraformaldehyde for 20 minutes, washed with PBS, and permeabilized with 0.5% Triton X-100 in PBS for 20 minutes. After washing with 0.05% Tween-20 in PBS, samples were blocked with PBS containing 1% to 2% BSA for 1 hour at room temperature. Cells were incubated with primary antibody for 16 to 24 hours at 4°C, followed by secondary antibodies (Alexa Fluor 488 or 594, 1:500; Thermo Fisher Scientific) for 1 to 2 hours at 37°C. The slides were washed with 0.05% Tween-20 in PBS and mounted with DAPI- or Hoechst containing medium. Images were acquired by a fluorescence microscope (TCS SP8, Leica) and analyzed by ImageJ (RRID: SCR_003070). Antibodies and their dilutions were listed in Supplementary Table S4.

Ki67 staining

Tumor sections (4 μm) were deparaffinized, blocked, and incubated with anti-Ki67 primary antibody (1:200; #16667, Abcam) at 4°C overnight. Signals were developed by IHC Select Immunoperoxidase Secondary Detection system (Merck Millipore) according to manufacturer's instructions. Hematoxylin was used for counterstaining and rabbit serum diluted to the same concentration of primary antibody was used as negative control. Images were captured by light microscope (Axio Imager 2, Zeiss) equipped with Metafer Automatic Slide Scanning and Imaging System (version 3.12.7; MetaSystems; RRID: SCR_016306). The proportion of Ki67-positive cells in each random field was measured by ImageJ (RRID: SCR_003070) with plugin IHC Profiler.

TUNEL staining

Tumor sections were deparaffinized, rehydrated, and fixed in 4% paraformaldehyde for 15 minutes. 100 μL of proteinase K (20 mg/mL) was added to each slide incubated at room temperature for 30 minutes. Upon PBS wash, 100 μL of equilibration buffer was added to each slide at room temperature for 10 minutes. Slides were then incubated at 37°C for 60 minutes after adding 100 μL of TdT reaction mix and being covered by plastic coverslips. Reaction was stopped by 2X SSC, and slides were blocked by 0.3% hydrogen peroxide for 5 minutes. 100 μL of streptavidin HRP (1:500 in PBS) was then added to each slide with incubation at room temperature for 30 minutes, followed by 100 μL of DAB solution for signal development.

Western blot

Cells were lysed using RIPA buffer or Tissue Protein Extraction Reagent (Thermo Fisher Scientific, 78510), and protein concentration was assessed using Pierce BCA Protein Assay Kit (Thermo Fisher Scientific, 23227). Proteins were separated using SDS-PAGE and transferred to PVDF membrane. The membrane was blocked using 5% BSA or milk, incubated with primary antibody, followed by washing and addition of horseradish peroxidase (HRP)-linked secondary antibody. Visualization was performed by chemiluminescent substrate (Thermo Fisher Scientific, 34096) in a ChemiDoc XRS+ Imaging System (Bio-Rad). Antibodies and their dilutions were listed in Supplementary Table S4.

Transwell migration and invasion assays

Transwell migration and invasion assays were performed using uncoated and Matrigel-coated Transwell chambers (8.0 μm pore size; Qiagen), respectively. Cells (1×10^6) was suspended in 200 μL of serum-free medium and seeded in the upper compartment. Complete culture medium containing 20% FBS (800 μL) was added to lower chamber. After 48 hours, migrated cells were washed with PBS, fixed in 4% paraformaldehyde for 15 minutes, and stained with crystal violet for 30 minutes. Three random fields were chosen to count the stained cells for statistical analysis.

Normal colonocytes culture

Murine colonic tissue specimens were collected from male mice aged 6 weeks at the Chinese University of Hong Kong. Normal epithelial cells were expanded in 3D culture in Matrigel (18). For cell viability, primary murine colonocytes were seeded in 96-well plate, transfected with siControl, siRUVBL1, and siRUVBL2 and cell viability was measured using CellTiter-Glo 3D Assay (Promega).

Organoid culture and YTHDF1 overexpression

Human colorectal cancer organoids were obtained from Princess Margaret Living Biobank. Organoids were embedded into Matrigel (Corning) and cultured in DMEM/F-12 (Gibco) with penicillin/streptomycin (100 U/mL), HEPES (10 mmol/L), Glutamax (Gibco), N2 supplement, B27 supplement, conditioned medium [containing WNT3A (50% v/v), R-spondin (10% v/v), Noggin (100 ng/mL)], EGF (50 ng/mL), FGF10 (1.25 mmol/L), gastrin (10 nmol/L), N-acetylcysteine (1.25 mmol/L), nicotinamide (10 mmol/L), A-83-01 (500 nmol/L; Tocris Bioscience), and SB202190 (1 μmol/L)). To overexpress YTHDF1, colorectal cancer organoids were transduced with YTHDF1 lentivirus. The growth of colorectal cancer

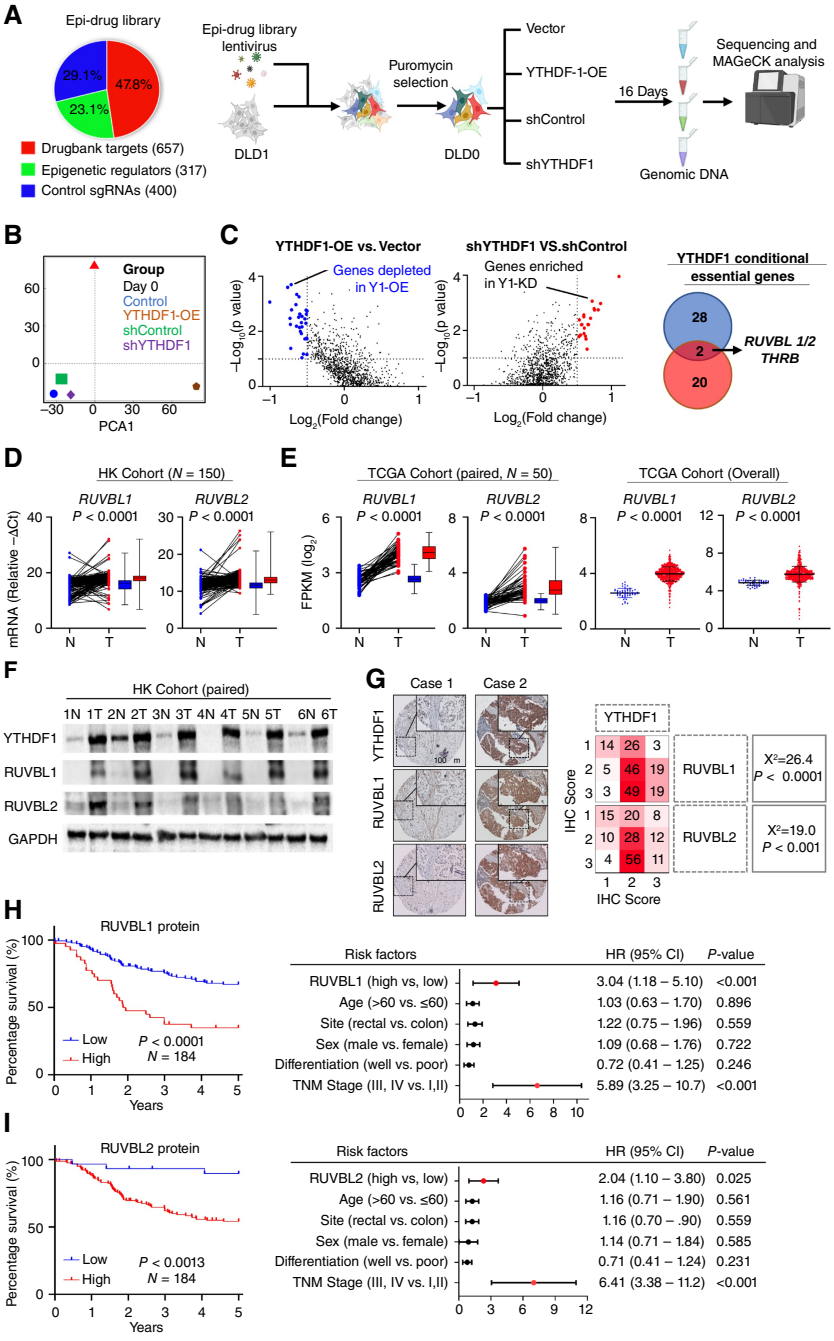

Figure 1.

Epi-Drug CRISPR dropout screens identify RUVBL1/2 as vulnerabilities of YTHDF1-expressing colorectal cancer cells. **A,** Composition of Epi-Drug sgRNA library and the workflow of CRISPR-Cas9 screens to identify YTHDF1-dependent vulnerabilities in colorectal cancer cells. **B,** Principal component analysis (PCA) of sgRNA abundances in each group at the end point of CRISPR-Cas9 screening. **C,** Left, top depleted genes in YTHDF1-overexpressing DLD1 cells vs. control vector ($\log_2$(fold change) < −0.5; $\log_{10}$(*P* value < −1). Middle, top enriched genes in shYTHDF1 cells vs. shControl ($\log_2$(fold change) > 0.5; $\log_{10}$(*P* value < −1). Right, overlapping of outlier genes identified the common candidates preferentially essential in a YTHDF1-dependent fashion. **D** and **E,** RUVBL1/2 mRNA expression in colorectal cancer cells compared with adjacent normal tissues in Hong Kong (**D**) and TCGA (**E**) colorectal cancer cohorts. In Hong Kong cohort, mRNA expression was normalized to β-actin. **F,** RUVBL1/2 and YTHDF1 proteins are overexpressed in colorectal cancer cells compared with paired adjacent normal tissues. **G,** Left, representative images of YTHDF1, RUVBL1, and RUVBL2 staining in colorectal cancer tissue microarrays (*N* = 184). Right, Pearson correlation analysis of YTHDF1, RUVBL1, and RUVBL2 protein expression. **H,** Left, Kaplan–Meier curve analysis of RUVBL1 protein expression and patient survival in colorectal cancer in tissue microarray cohort (*N* = 184). Right, multivariate Cox regression analysis. RUVBL1-low, IHC score 1; RUVBL1-high, IHC score 2 to 3. **I,** Left, Kaplan–Meier curve analysis of RUVBL2 protein expression and colorectal cancer patient survival. Right, multivariate Cox regression analysis. RUVBL2-low, IHC score 1 to 2; RUVBL2-high, IHC score 3. Paired *t* test (**D** and **E**; left), Student *t*-test (**E**; right), Pearson χ^2 test (**G**), or log rank test (**H** and **I**).

organoids was captured in an inverted light microscope and the surface area of organoids in each random field was measured by ImageJ (version 1.53a; RRID: SCR_003070).

Measurement of liver or kidney function indicators

Creatinine, blood urea nitrogen, alanine aminotransferase, and aspartate transaminase were measured in serum from the VNP-treated animals, using Catalyst One Chemistry Analyzer (IDEXX) following the instructions from the user manual. 40 μL of each serum sample were diluted with PBS to a total volume of 120 μL, and then loaded to specific catalyst slides. The slides were then read with the analyzer automatically.

Subcutaneous xenograft assay

DLD1 and HCT116 cells (5×10^6 cells, 0.1 mL PBS) overexpressing vector or YTHDF1, with or without RUVBL1/2 knockout were subcutaneously injected into both flanks of 6-week-old female BALB/c nude mice ($n = 6$–8 tumors/group), respectively. Tumor size was measured twice a week using a digital caliper. Tumor volume (mm^3) was estimated as follows: $V = 0.5 \times L \times W^2$, in which L: the longest diameter, and W: shortest diameter (W). At sacrifice, tumors were weighed and stored in −80°C or 10% formalin for further analysis. All animal experiments were approved by the Animal Experimentation Ethics Committee of the Chinese University of Hong Kong (Ref. No. 19-205).

Colon-specific *Ythdf1* knockin mice

Conditional *Ythdf1* knockin mice ($Rosa26^{lsl\text{-}Ythdf1}$) was generated by Shanghai Model Organisms Center (Shanghai, China) and crossed with CDX2-Cre^{ERT2} mice to establish intestine-specific *Ythdf1* knockin mice ($Rosa26^{lsl\text{-}Ythdf1}$CDX2-$Cre^{ERT2}$). At 6 to 8 weeks old, mice were intraperitoneally injected with a single dose of tamoxifen (100 mg/kg) to activate *Ythdf1* overexpression as described (9). All animal experiments were approved by the Animal Experimentation Ethics Committee of the Chinese University of Hong Kong (Ref. No. 19-205).

Methylated RNA immunoprecipitation-qPCR

Total RNA was extracted with TRIzol reagent. DNA contamination was removed using DNase (Takara, RR037B), and RNA was fragmented with RNA Fragmentation Buffer (10 mmol/L Tris-HCl, 10 mmol/L $ZnCl_2$) for 5 minutes at 70°C. Fragmented RNA was pulled down by incubation with anti-m^6A antibody (Abcam, ab208577) and Protein A/G Magnetic Beads (MedChemExpress, HY-K0202) at 4°C for 4 hours in the presence of RNase inhibitor (Thermo Fisher Scientific, 10777019). Beads were then washed twice in IP buffer (150 mmol/L NaCl, 10 mmol/L Tris-HCl, pH 7.5, 0.1% IGEPAL CA-630), low-salt IP buffer (50 mmol/L NaCl, 10 mmol/L Tris-HCl, pH 7.5, 0.1% IGEPAL CA-630), and high-salt IP buffer (500 mmol/L NaCl, 10 mmol/L Tris-HCl, pH 7.5, 0.1% IGEPAL CA-630), respectively. RNA was eluted using RLT buffer (QIAGEN, 74106) and purified with DireCTzol RNA Miniprep Kit (Zymo Research, R2050). Isolated RNAs were reverse-transcribed and analyzed by qPCR.

RNA immunoprecipitation qPCR

RNA immunoprecipitation (RIP) was performed using anti-YTHDF1 antibody (Proteintech, 26787-1-AP) and EZ-Magna RIP RNA-Binding Protein Immunoprecipitation Kit (Sigma, 17-701). Briefly, cells were lysed with RIP Lysis Buffer, and lysates were incubated with magnetic beads bound with the anti-YTHDF1 antibody overnight at 4°C. Beads were then washed with RIP Wash Buffer for six times, and RNA was released by proteinase K digestion in SDS (1%, w/v) at 55°C for 30 minutes. RNA was isolated by phenol:chloroform: isoamyl alcohol (Fisher Scientific, BP1754I) and precipitated by ethanol. Isolated RNAs were reverse-transcribed and analyzed by qPCR.

Ribosome-nascent chain complex qPCR

Cells were preincubated with 100 mg/mL of cycloheximide for 15 minutes, rinsed with PBS and lysed in ribosome buffer (20 mmol/L HEPES-KOH, pH 7.4, 15 mmol/L $MgCl_2$, 200 mmol/L KCl, 100 mg/mL cycloheximide, and 2 mmol/L dithiothreitol) containing 1% Triton X-100. After 30 minutes incubation on ice, cell lysates were scraped and centrifuged at 16,200 *g* for 10 minutes at 4°C. Supernatants were transferred 10 mL of sucrose buffer (30% sucrose in RB buffer). Ribosome-nascent chain complexes (RNC) were pelleted after ultracentrifugation at 185,000 *g* for 5 hours at 4°C. Total RNA and RNC-RNA were respectively isolated by using TRIzol reagent. Isolated RNAs were reverse-transcribed and analyzed by qPCR.

Polysome profiling analysis

Cells were treated with 100 μg/mL cycloheximide (Sigma) for 15 minutes at 37°C, lysed on ice, and centrifuged at 13,000 *g* for 10 minutes at 4°C. Sucrose gradient centrifugation (10%–50%, w/v) was performed in SW41 ultracentrifuge tubes (Backman) for 3 hours at 38,000 *g* 4°C in an SW41 rotor. Gradients were fractionated at absorbance 254 nm (Bio-Rad). Nonribosome (<40S), 40S, 60S, 80S and the polysome fractions were pooled and total RNA was isolated using TRIzol reagent for downstream analysis.

Luciferase reporter assay

Cells were cotransfected with pmiRGLO-RUVBL1/2- 3′UTR or pmiRGLO-RUVBL 1/2-Mut-3′ UTR in a 12-well plate, together with pRL-TK (RRID: Addgene_11313). At 24 hours post-transfection, cells were lysed (Promega, E3971) and analyzed with the Dual-Glo Luciferase Assay (Promega). Luciferase (F-luc) activity was normalized to *Renilla* (R-luc) activity.

Homopropargylglycine assay

Nascent protein synthesis was detected by using Click-iT HPG Alexa Fluor 594 Protein Synthesis Assay Kit (Thermo Fisher Scientific, C10429). Cells were cultured in l-methionine-free medium with L-homopropargylglycine (HPG) at 37°C for 30 minutes. Cells were then washed with PBS, fixed by 3.7% formaldehyde for 15 minutes, and permeabilized with 0.5% Triton X-100 for 15 minutes. Next, Click-iT reaction cocktail was added for 30 minutes. After nuclear staining, imaging analysis was performed by a fluorescence microscope.

Puromycin incorporation assay

Cells were seeded in six-well plates (3×10^5 cells/per well). At the end point, cells were incubated with puromycin (1 μg/mL) for 30 to 60 minutes, and then lysed in RIPA buffer. The lysate was separated on SDS-PAGE, transferred to PVDF membrane and then detected with anti-puromycin antibody. A loading control gel was run in parallel and stained with Coomassie Blue solution.

Immunohistochemistry

Paraffin embedded tissues were sectioned, deparaffinized, and rehydrated. Antigens were then retrieved with sodium citrate buffer (10 mmol/L sodium citrate, 0.05% Tween 20, pH 6.0), and the

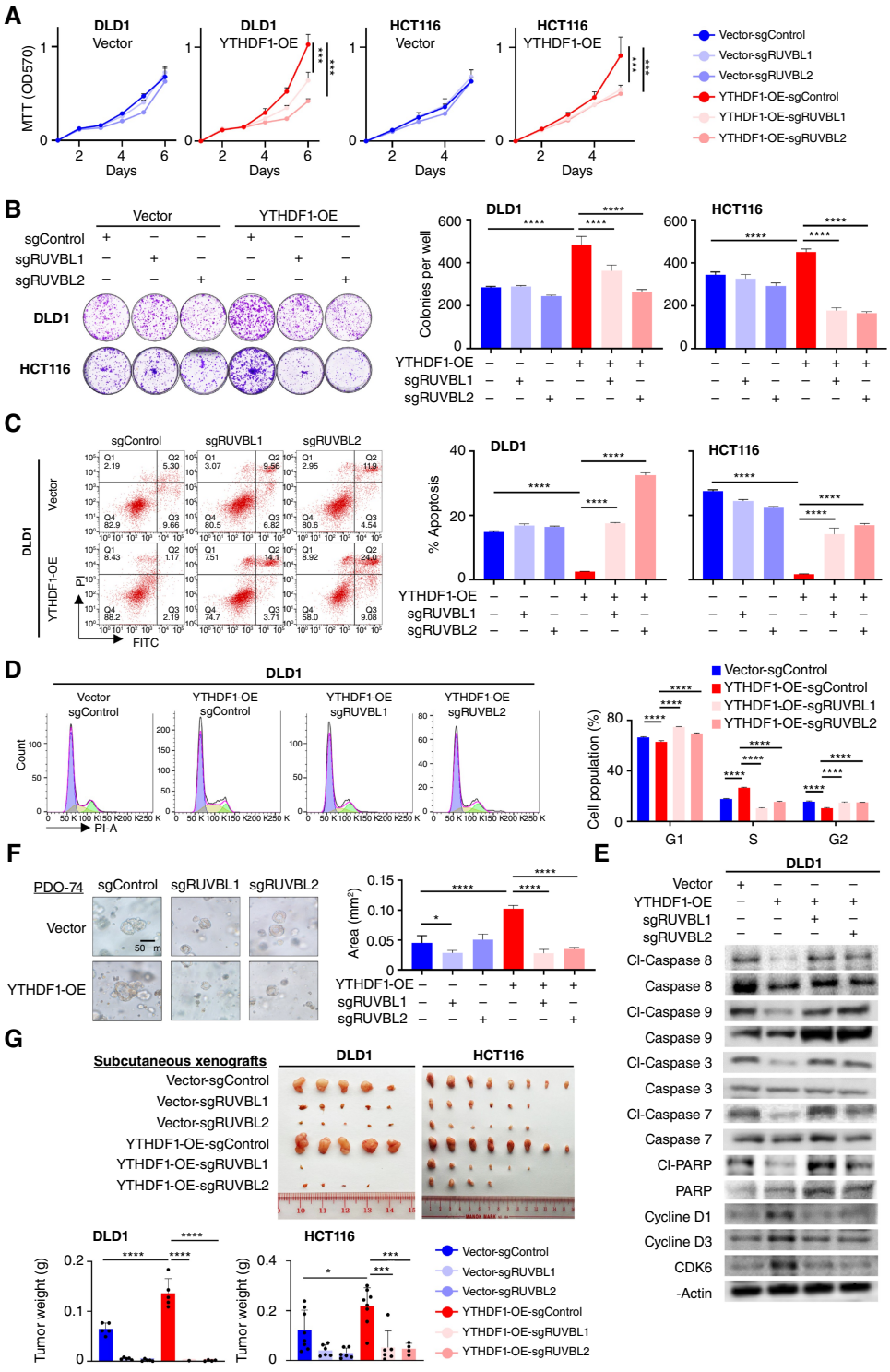

Figure 2.

RUVBL1/2 knockout abolishes oncogenic function of YTHDF1 *in vitro* and *in vivo*. **A–D,** Effect of RUVBL1/2 knockout on vector- and YTHDF1-overexpressing DLD1 and HCT116 cell proliferation ($N = 10$; **A**), colony formation ($N = 3$, 7–14 days; **B**), apoptosis ($N = 3$; **C**), and G_1-S cell cycle transition ($N = 3$; **D**). **E,** Western blot of cell cycle and apoptosis markers. **F,** Representative brightfield images of primary colorectal cancer tumor-derived organoids expressing vector or YTHDF1, with or without RUVBL1/2 knockout. **G,** Effect of RUVBL1/2 knockout on vector- and YTHDF1-overexpressing DLD1 and HCT116 xenografts in nude mice. RUVBL1/2 abrogated differential growth between vector- and YTHDF1-overexpresing xenografts (DLD1, $N = 5$; HCT116, $N = 8$). Two-way ANOVA (**A**) and one-way ANOVA (**B–D** and **G**). *, $P < 0.05$; **, $P < 0.01$; ***, $P < 0.001$; ****, $P < 0.0001$.

sections were treated with 3% H_2O_2 and blocked with 5% goat serum. Sections were incubated with anti-RUVBL1, anti-RUVBL2, or anti-YTHDF1 overnight at 4°C, followed by incubation with goat anti-rabbit IgG-HRP conjugate (Bio-Rad, 1706515). Sections were counterstained with hematoxylin. Images were acquired using a light microscope and scored by a pathologist blinded to the nature of the samples. IHC score 1: <10% staining; IHC score 2: ≤70% weak or moderate staining or strong staining in 10% to 30%; IHC score 3: moderate staining in >70% or strong staining in >30%. Antibodies and their dilutions were listed in Supplementary Table S4.

Coimmunoprecipitation and mass spectrometry

Cells were lysed in RIPA buffer. For coimmunoprecipitation, 1 mg tissue lysates were incubated with 1 μg anti-YTHDF1, anti-RUVBL1, anti-RUVBL2, anti-Flag, or normal IgG overnight at 4°C. To perform pulldown, the mixture was incubated in 50 μL Protein A/G Mix Magnetic Beads (Merch Millipore) for 1 hour at 4°C. The beads were washed using RIPA buffer, and proteins were eluted by heating in SDS-PAGE loading buffer. Eluted proteins were separated by SDS-PAGE and analyzed by silver staining (Thermo Fisher Scientific 24612). For recombinant protein pulldown, human YTHDF1 (Origene, TP307185L), RUVBL1 (Origene, TP301170), RUVBL2 (Origene, TP300933) proteins (2 μg) were incubated in stock buffer (50 mmol/L Tris-Cl, 150 mmol/L NaCl, pH 8.0) for overnight at 4°C, followed by pulldown assays as described above. For MS analysis, the silver-stained bands were excised, trypsin digested, and analyzed by nano-UPLC (EASY-LC1200) coupled to a Q Exactive HFX Orbitrap MS (Thermo Fisher Scientific). Raw MS files were processed using Proteome Discoverer software (ver2.4.0.305; RRID: SCR_014477) and built-in Sequest HT search engine (19) using UniProt FASTA databases (RRID:SCR_002380). A maximum of two missed cleavage(s) was allowed. FDR was set to 0.01. Other parameters were set as default. Enrichment of GO biological process terms for protein candidates was assessed using topGO package (RRID:SCR_014798) in R (20). Gene set enrichment analysis (GSEA) was performed in GSEA software (21), and queried against Kyoto Encyclopedia of Genes and Genomes (KEGG) MEDICUS pathway database (619 gene sets).

Ribosome sequencing

Cells were treated with 100 μg/mL cycloheximide for 5 minutes at 37°C, and unprotected mRNA regions in cells digested with RNase I. Ribosome sequencing (Ribo-seq) was performed by Omicsmart. Intact mRNA-ribosome complexes were sequenced using illumina HiSeq 4000. Reads mapped to human rRNAs, snoRNAs, snRNAs, and tRNAs were excluded, and residual reads were mapped to human genome via bowtie2 (v2.3.4.3; RRID: SCR_005476; ref. 22). Feature–Counts (v1.6.4; ref. 23) with the following parameters (M–fracOverlap 0.4–largestOverlap) was used for calculating the expression of protein-coding genes. GSEA was performed in GSEA software (21), and queried against KEGG MEDICUS pathway database (619 gene sets). Genes were ranked by the signal-to-noise method. Enrichment scores and *P* values were calculated using default parameters. To estimate the translation efficiency (TE), RNA-seq was performed with total RNA, and libraries were sequenced using illumina HiSeq 4000 (PE150). FPKM (fragments per kilobase of transcript per million mapped reads) was calculated using DESeq2 (RRID: SCR_000154; ref. 24). Integrative genomics viewer was used to display TE as enrichment ratio of Ribo-seq to RNA-seq.

Vesicle-like PLGA-based nanoparticle formulation and treatment

Vesicle-like PLGA-based nanoparticles (VNP) were assembled by Kelan Biotechnology Co. Ltd. siRNAs with 2′-O-methyl (2′-OMe) modification were purchased from GenePharma Co. Ltd. The sequences of human *RUVBL1* siRNAs were as follow: sense: GCCAGCUAAUGAAGCCAAATT, antisense: UUUGGC-UUCAUUAGCUGGCTT; human *RUVBL2* siRNAs were sense: CCGGAGAUCCGUGAUGUAATT, antisense: UUACAUCAC-GGAUCUCCGGTT. For drug treatment, DLD1 or HCT116 xenografts (5×10^6 cells/tumor) were injected into both flanks of NSG mice. When tumor reached 50 to 100 mm^3, mice were randomized ($N = 6$ tumors per group) and then treated with VNP-siNC, VNP-siRUVBL1, and VNP-siRUVBL2 via intratumoral injection (2 mg/kg) twice a week. All animal experiments were approved by the Animal Experimentation Ethics Committee of the Chinese University of Hong Kong (Ref. No. 19-205).

Statistical analysis

All measurements were acquired using independent samples. GraphPad Prism version 8 (GraphPad Software; RRID: SCR_002798) was used for data analysis, and the data were shown as means ± SD, unless stated otherwise. Two-tailed Student *t* test was used for statistical analysis between two groups, unless stated otherwise. One-way ANOVA was used for comparisons between more than two groups. A *P* value <0.05 was considered as statistically significant.

Data availability

The Ribo-seq data generated in this study are publicly available in the SRA database at PRJNA1121114. All other data are available upon request from the corresponding author. The TCGA colorectal cancer (GDC COAD and GDC READ) data analyzed in this study were obtained from the UCSC Xenabrowser at https://xena.ucsc.edu/. The DepMap data analyzed in this study were obtained from the online DepMap portal at https://depmap.org/portal/.

Results

Epi-drug CRISPR/Cas9 screening identifies RUVBL1/2 as genetic vulnerabilities of YTHDF1-overexpressing colorectal cancer

To screen for druggable genes that preferentially suppresses YTHDF1-overexpressing colorectal cancer, we used Epi-Drug library, an inhouse CRISPR/Cas9 sgRNA library comprising ~12,500 sgRNAs targeting 657 Drugbank-based targets and 317 epigenetic regulators (**Fig. 1A**). DLD1 harboring the Epi-Drug library were transduced with lentivirus to overexpress or knockdown YTHDF1, followed by 16 days continuous culture (**Fig. 1A**). Principal component analysis showed that DLD1 cells with high YTHDF1 were separated from other groups, whereas the DLD1 controls were clustered together (**Fig. 1B**). We focused on genes that were preferentially depleted in YTHDF1-overexpressing cells (YTHDF1-OE vs. vector); while simultaneously being enriched when YTHDF1 was depleted (shYTHDF1 vs. shControl; **Fig. 1C**). Overlapping of these gene candidates resulted in the identification of RUVBL1/2 and THRB as potential targets for YTHDF1-expressing colorectal cancer cells (**Fig. 1C**). These results thus identified preferential essential genes in the context of YTHDF1-high colorectal cancer. Consistent with our results, the analysis of DepMap dataset demonstrated that RUVBL1/2 knockout gene effect scores negatively correlated with YTHDF1 copy number in a panel of colorectal cancer cell lines ($n = 58$;

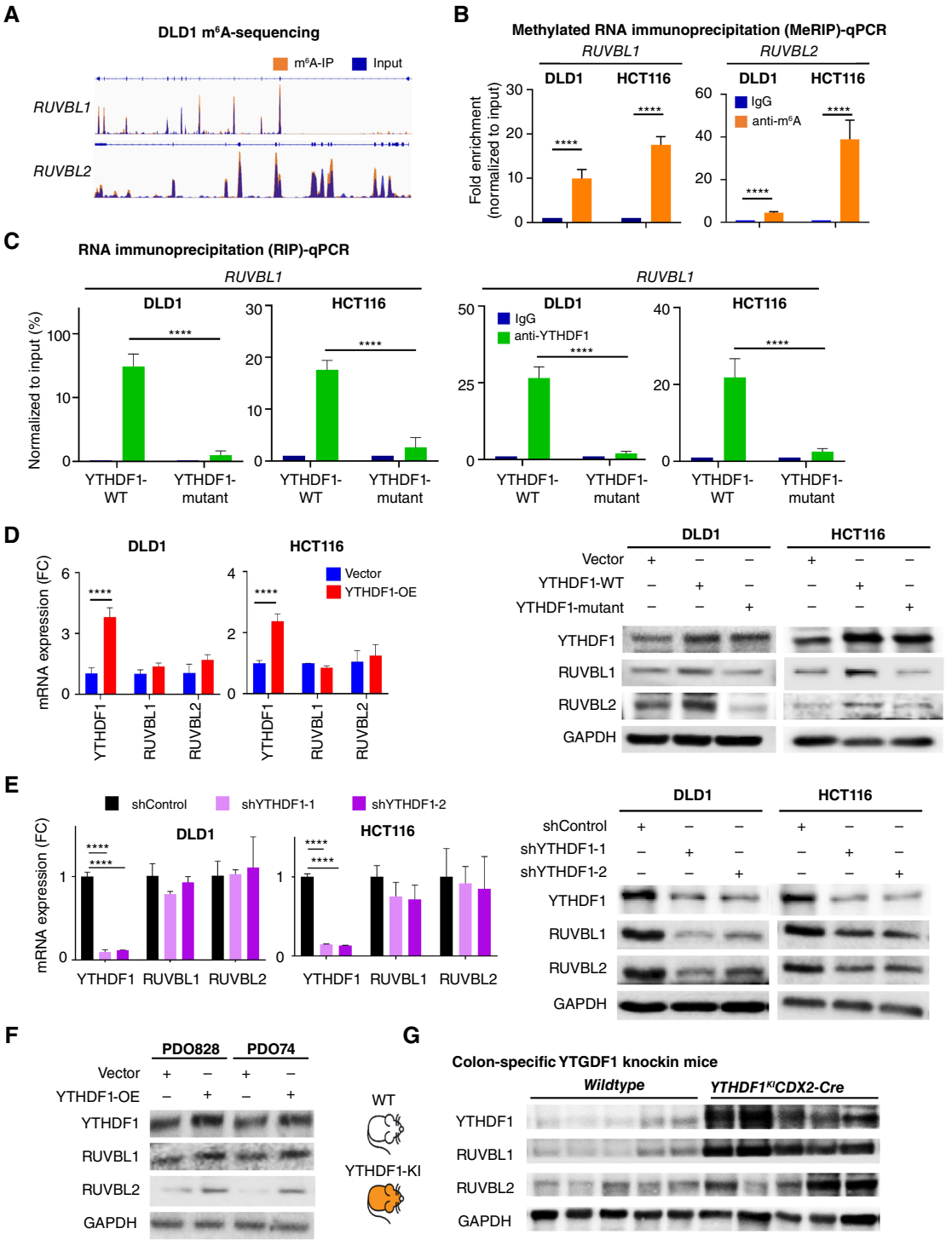

Figure 3.

YTHDF1 directly targets m^{6}A-modified RUVBL1/2 mRNA methylation and promotes their protein expression *in vitro* and *in vivo*. **A,** UCSC snapshots of m^{6}A-seq reads of RUVBL1/2 mRNA in DLD1 cells. The normalized read densities are shown for m^{6}A (orange) and input (blue). **B,** Methylated RIP-qPCR analysis of m^{6}A-modified RUVBL1/2 mRNA in DLD1 and HCT116 cells. **C,** RIP-qPCR with anti-YTHDF1 antibody showed binding of YTHDF1 to RUVBL1/2 mRNA, whereas mutant YTHDF1 (K395A, Y397A) had attenuated binding. **D** and **E,** Effect of YTHDF1 overexpression (**D**) or knockdown (**E**) on RUVBL1/2 mRNA and protein expression in DLD1 and HCT116 cells. **F,** Effect of YTHDF1 overexpression on RUVBL1/2 protein expression in primary colorectal cancer organoids PDO828 and PDO74. **G,** Expression of YTHDF1 and RUVBL1/2 in intestinal-specific Ythdf1 knockin mice (Ythdf1^{lsl}Cdx2-Cre^{ERT2}) as compared with wildtype mice. Student *t* test (**B–D**) and one-way ANOVA (**E**). ****, $P < 0.0001$.

Supplementary Fig. S1A), implying RUVBL1/2 knockout caused a greater depletion of YTHDF1-high colorectal cancer cells. Meanwhile, mutations in APC, KRAS, TP53, or FBXW7 had no effect (Supplementary Fig. S1B).

RUVBL1/2 are overexpressed in colorectal cancer patients and predict poor survival

To ask if RUVBL1/2 are potential oncogenic factors in colorectal cancer, we examined its clinical significance in independent colorectal cancer patient cohorts. We first examined mRNA expression of RUVBL1/2 in our colorectal cancer cohort ($n = 150$), showing that both are upregulated in colorectal cancer compared with paired adjacent normal tissues (both $P < 0.0001$; **Fig. 1D**). Consistently, RUVBL1/2 mRNA was overexpressed in colorectal cancer from TCGA dataset (both $P < 0.0001$; **Fig. 1E**). Western blot further confirmed that YTHDF1 and RUVBL1/2 were all upregulated in colorectal cancer compared with paired adjacent normal tissues (**Fig. 1F**). The correlation between YTHDF1 and RUVBL1/2, protein expression was then determined in a TMA cohort ($n = 184$). Positive correlations were found between YTHDF1 and RUVBL1 ($\chi^2 = 26.4$; $P < 0.0001$) or RUVBL2 ($\chi^2 = 19$; $P < 0.001$) protein expression in TMA cohort by IHC (**Fig. 1G**; Supplementary Fig. S2A). Moreover, survival analysis based on TMA cohort ($n = 184$) showed that protein expression of RUVBL1 ($P = 0.0041$) and RUBVL2 ($P = 0.0025$) were both correlated to poor survival of colorectal cancer patients (**Fig. 1H** and **I**). In the TCGA cohort, higher mRNA expression of RUVBL1 also correlated with poor survival in colorectal cancer (Supplementary Fig. S2B). Multivariate Cox regression analysis was performed next to investigate the significance of RUVBL1/2 protein on prognosis of colorectal cancer patients in conjunction with clinicopathological features, including age, sex, tumor site, tumor differentiation, and TNM stage. Either high RUVBL1 or RUVBL2 protein expression were independent prognostic factor for colorectal cancer [RUVBL1:HR = 3.04, 95% confidence interval (CI) = 1.18–5.10, $P < 0.001$; RUVBL2:HR = 2.04, 95% CI = 1.10–3.80, $P < 0.05$]. Our results demonstrated that RUVBL1/2 are overexpressed in colorectal cancer and predict poor prognosis in colorectal cancer patients.

RUVBL1/2 knockout abrogates oncogenic function of YTHDF1 in colorectal cancer cells

RUVBL1 and RUVBL2 are known to assemble into a dimer to perform their functions, such as ATPase activity (25, 26). We thus examined their roles by knockout of RUVBL1 or RUVBL2 in colorectal cancer cells with YTHDF1-OE (Supplementary Fig. S3A). In DLD1 and HCT116 cells, YTHDF1 overexpression promoted cell viability and colony formation (**Fig. 2A** and **B**). Our results showed that RUVBL1/2 knockout impaired cell viability of DLD1 and HCT116 cells with YTHDF1-OE (both $P < 0.001$), while having no effect on respective control cells (**Fig. 2A**). Colony formation assay also showed that RUVBL1/2 knockout preferentially suppressed colony growth ($P < 0.001$) in YTHDF1-OE DLD1 and HCT116 cells (**Fig. 2B**). Besides, in a panel of colorectal cancer cells with diploid YTHDF1 or with YTHDF1 gene amplification, siRUVBL1/2 also preferentially suppressed growth of YTHDF1-amplified colorectal cancer cells (Supplementary Fig. S3B–S3D). siRUVBL1/2 did not exert growth inhibitory effects on normal colonic NCM460 cells and mouse primary normal colonocytes (Supplementary Fig. S3B–S3D), suggesting that RUVBL1/2 is a preferential therapeutic target in YTHDF1-high colorectal cancer cells.

We next investigated the interplay between YTHDF1 and RUVBL1/2 in apoptosis and cell cycle progression. In DLD1 and HCT116 cells, YTHDF1-OE abolished Annexin V^+ apoptotic cells (**Fig. 2C**), while RUVBL1/2 knockout restored apoptosis to that of control cells (**Fig. 2C**). Similarly, RUVBL1/2 depletion reversed the effect of YTDHF1-OE on promoting G_1-S cell cycle progression (**Fig. 2D**). To validate these observations, we then performed Western blot of apoptosis and cell cycle markers. Indeed, RUVBL1/2 knockout restored apoptosis in YTHDF1-OE cells, as evidenced by the increased expression of cleaved caspase-9, caspase-8, caspase-3, caspase-7, and PARP (**Fig. 2E**). Cyclin D1, cyclin D3, and CDK6, G_1-S cell cycle progression markers induced by YTHDF1, were downregulated following RUVBL1/2 knockout (**Fig. 2E**). RUVBL1/2 knockout also inhibited YTHDF1-OE induced cell migration and invasion (Supplementary Fig. S4A and S4B).

To validate our observations in colorectal cancer cell lines, we overexpressed YTDHF1 in PDO74, a primary colorectal cancer patient-derived tumor organoid. YTHDF1 overexpression increased the outgrowth of PDO74 organoids, which was abolished by RUVBL1/2 knockout (**Fig. 2F**). Moreover, we performed *in vivo* subcutaneous xenograft studies in nude mice with DLD1 and HCT116 cells (**Fig. 2G**). In both DLD1 and HCT116 xenograft models, the overexpression of YTHDF1 promoted tumor growth *in vivo*, but their growth was significantly impaired by RUVBL1/2 knockout (all $P < 0.001$; **Fig. 2G**). Strikingly, knockout of RUVBL1 (4 out of 5) and RUVBL2 (1 out of 5) prevented tumor initiation in YTHDF1-overexpressing DLD1 xenografts, but not in DLD1-sgControls (**Fig. 2G**). In HCT116 xenografts, RUVBL1/2 knockout also abrogated induction of tumor growth by YTHDF1 (**Fig. 2G**). Together, *in vitro* and *in vivo* evidence demonstrated that the depletion of RUVBL1/2 preferentially targets YTHDF1-overexpressing cells, thereby abolishing the oncogenic role of YTHDF1 in colorectal cancer.

RUVBL1/2 mRNAs are m^6A-modified and are direct targets of YTHDF1

In light of the association between RUVBL1/2 and YTHDF1 expression in colorectal cancer patient cohorts (**Fig. 1**) and the functional dependence of YTHDF1 on RUVBL1/2 (**Fig. 1**), we next investigated if RUVBL1/2 are molecular targets of YTHDF1. We performed m^6A-sequencing of DLD1 cells, which revealed that both RUVBL1/2 mRNA were m^6A-modified (**Fig. 3A**), which was further validated by m^6A methylated RIP-qPCR analysis (**Fig. 3B**). Next, we asked if YTHDF1 recognizes m^6A-modified RUVBL1/2 mRNA. Interplay between RUVBL1/2 mRNA and YTHDF1 was determined by RIP-qPCR (**Fig. 3C**). We performed RIP-qPCR with anti-YTHDF1 in DLD1 and HCT116 cells with the overexpression of wildtype YTHDF1 or mutant YTHDF1 (K395A, Y397A) defective in binding to m^6A-modified mRNA. In both cell lines, RUVBL1/2 mRNA was pulled down by wildtype YTHDF1 but not its mutant counterpart (**Fig. 3C**), inferring that YTHDF1 binds to RUVBL1/2 mRNA in a m^6A-dependent fashion.

YTHDF1 induces protein expression of RUVBL1/2 by boosting their translation

Next, we determined the effect of YTHDF1 on RUVBL1/2 expression. Ectopic expression of YTHDF1 in DLD1 and HCT116 cells had no effect on RUVBL1/2 mRNA (**Fig. 3D**). Overexpression of wildtype YTHDF1, but not mutant YTHDF1, induced protein expression of RUVBL1/2 in these cells (**Fig. 3D**). Conversely,

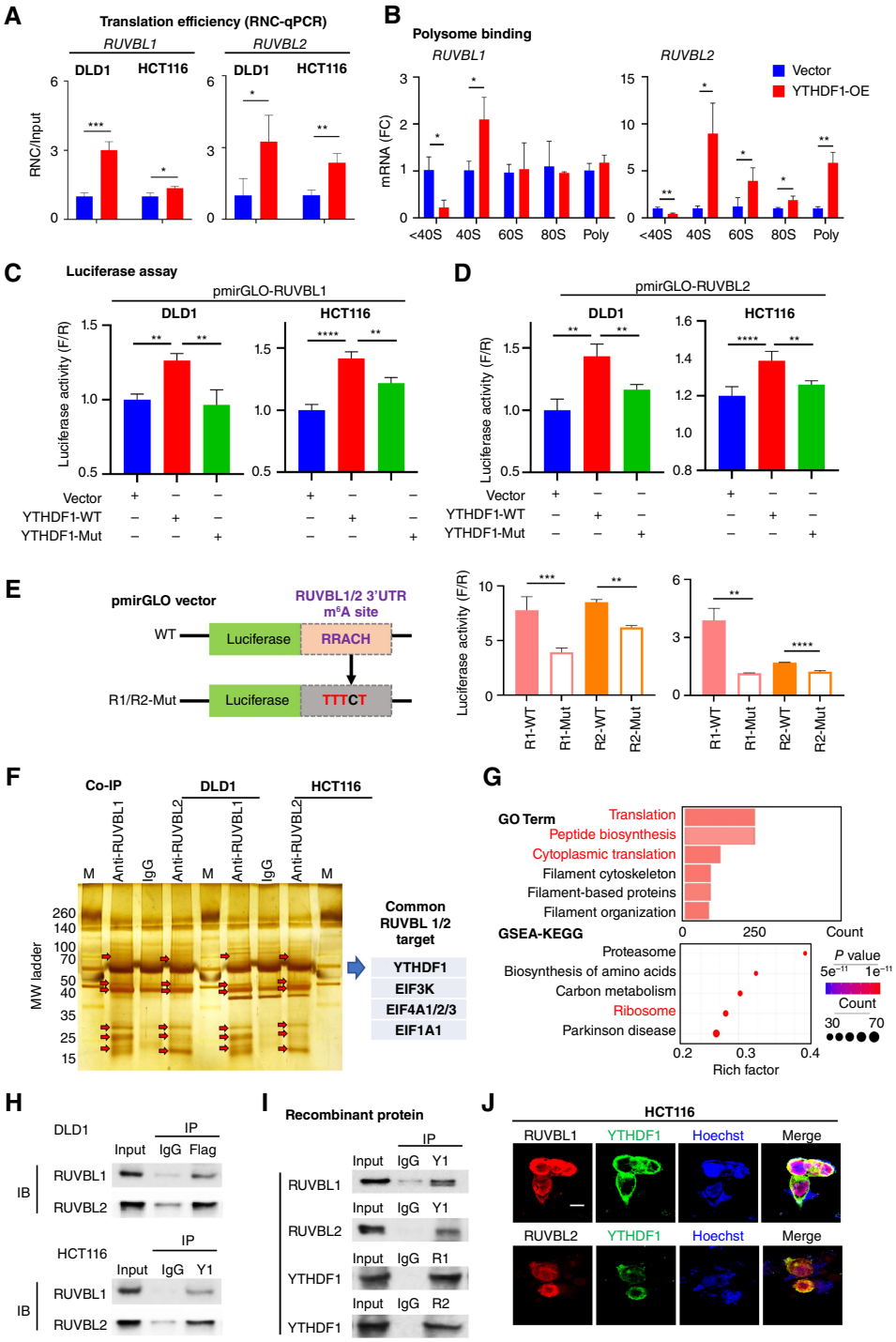

Figure 4.

YTHDF1 promotes translation efficiency of RUVBL1/2, which in turn interact with YTHDF1 and translational initiation factors. **A,** RNC-qPCR analysis of ribosome-associated RUVBL1/2 mRNA in vector- and YTHDF1-overexpressing DLD1 and HCT116 cells. **B,** Enrichment of RUVBL1/2 mRNA in <40S, 40S, 60S, 80S, and polysomes from HCT116 cells with or without YTHDF1 overexpression. **C** and **D,** Colorectal cancer cells overexpressing wildtype YTHDF1 or mutant YTHDF1 were transfected with pmirGLO-RUVBL1 (**C**) or pmirGLO-RUVBL2 (**D**) containing respective 3′UTR sequences, followed by luciferase assays. **E,** pmirGLO-RUVBL1/2-mutant reporters with mutated m^6A sites (RRACH to TTTCT) in the 3′UTR region demonstrated decreased luciferase activity. **F,** RUVBL1/2 coimmunoprecipitation and mass spectrometry for identification of common interacting proteins. **G,** Pathway enrichment analysis [gene ontology (GO), GSEA-KEGG] of interacting partners of RUVBL1/2. **H,** Coimmunoprecipitation by anti-YTHDF1 verified binding of YTHDF1 to RUVBL1/2. **I,** Coimmunoprecipitation using recombinant YTHDF1 and RUVBL1/2 confirmed direct protein–protein interplay between YTHDF1 and RUVBL1/2. **J,** Colocalization of RUVBL1/2 and YTHDF1 in HCT116 cells was determined by immunofluorescence staining. Student *t* test (**A**, **B**, and **E**) and one-way ANOVA (**C** and **D**). *, $P < 0.05$; **, $P < 0.01$; ***, $P < 0.001$; ****, $P < 0.0001$.

knockdown of YTHDF1 in colorectal cancer cells did not affect RUVBL1/2 mRNA, but it significantly reduced their protein expression (**Fig. 3E**), suggesting that YTHDF1 impacts RUVBL1/2 protein translation. Similar to that in colorectal cancer cells, YTHDF1 overexpression in two primary colorectal cancer organoids PDO74 and PDO828 elevated RUVBL1/2 protein expression (**Fig. 3F**). To corroborate these findings *in vivo*, we examined the expression of RUVBL1/2 in intestine-specific, YTHDF1 knockin mice ($Ythdf1^{lsl}Cdx2\text{-}Cre^{ERT2}$; ref. 9). Western blot of colonic tissues showed that RUVBL1/2 were both upregulated in YTHDF1 knockin mice as compared with wildtype littermates (**Fig. 3G**).

To investigate whether YTHDF1 promoted translation of RUVBL1/2, we measured ribosome-associated RUVBL1/2 mRNA and performed ribosome-nascent chain complex (RNC)-qPCR, which showed that YTHDF1 overexpression increased RUVBL1/2 mRNA in ribosomes of DLD1 and HCT116 cells (**Fig. 4A**). We further separated ribosomal RNAs into different fractions—untranslated (<40S), translation initiation (40S, 60S, 80S ribosomes), and translationally active polysomes (>80S)—in cells overexpressing control vector or YTHDF1 (**Fig. 4B**). In the YTHDF1-OE group, RUVBL1 mRNA was significantly decreased in untranslated fraction (<40S), with a corresponding increase in 40S fraction, indicative of increased translation initiation (**Fig. 4B**). The untranslated fraction of RUVBL2 was also reduced by YTHDF1 overexpression, together with enrichment in both 40S-80S monomer, as well as polysomes. These findings indicate the association of RUVBL1/2 mRNA with active translating ribosomes upon YTHDF1 overexpression. We next constructed the luciferase reporters for RUVBL1/2 translation by linking their 3′UTR sequences to the pmirGLO vector. As shown in **Fig. 4C** and **D**, YTHDF1 overexpression increased luciferase activities of both RUVBL1/2 reporters in DLD1 and HCT116 cells, whereas mutant YTHDF1 had no equivalent effects. Finally, we generated RUVBL1/2 luciferase vectors with 3′UTR with mutated m^6A motif (RRACH to TTTCT; **Fig. 4E**). RUVBL1/2 m^6A mutants demonstrated decreased luciferase activities in YTHDF1-overexpressing colorectal cancer cells (**Fig. 4E**). Collectively, YTHDF1 overexpression promoted translation and protein expression of RUVBL1/2 in a m^6A-depdendent manner.

RUVBL1/2 protein directly interacts with YTHDF1 in association with translation initiation complex

Next, we aimed to decipher molecular mechanisms whereby RUVBL1/2 depletion could preferentially suppress YTHDF1-high colorectal cancer. To this end, we determined interactome of RUVBL1/2 using coimmunoprecipitation assay with anti-RUVBL1 or anti-RUVBL2, followed by LC-MS/MS analysis of enriched protein bands (**Fig. 4F**). The overlap of protein candidates identified by mass spectrometry demonstrated numerous common protein candidates as binding partners of RUVBL1/2 (**Fig. 4F**), including YTHDF1, EIF3K, EIF4A, and EEF1A1. The GO and GSEA-KEGG analyses showed that the interactome of RUVBL1/2 was enriched with translation-related pathways, including translation, peptide biosynthetic, cytoplasmic translation, and ribosome (**Fig. 4G**). To validate this, we performed reciprocal co-immunoprecipitation assay with pulldown of YTHDF1 in DLD1 and HCT116 cells, which unraveled RUVBL1/2 as protein partners (**Fig. 4H**). Next, we performed coimmunoprecipitation with recombinant YTHDF1 and RUVBL1/2 proteins (**Fig. 4I**), confirming the direct protein–protein interactions between YTHDF1 and RUVBL1/2. Coimmunofluorescence staining of YTHDF1 with RUVBL1/2 demonstrated the co-localization of these proteins in HCT116 cells (**Fig. 4J**). RUVBL1/2 and YTHDF1 also interact with other candidates related to translation initiation (EIF3K and EIF4A; Supplementary Fig. S5A and S5B). Taken together, it indicates RUVBL1/2 binds to YTHDF1, which in turn are associated with translation initiation complex.

RUVBL1/2 knockout impairs YTHDF1-mediated translation initiation

Because YTHDF1 modulates TE of its target m^6A-modified mRNA by interacting with key translation initiation factors (3), we propose a hypothesis that YTHDF1 and RUVBL1/2 form a positive feedforward cycle, whereby YTHDF1 upregulates RUVBL1/2 translation, which functions as essential components of YTHDF1-induced translation initiation complexes that boosts the translation of YTHDF1 targets. We thus evaluated the effect of RUVBL1/2 knockout on YTHDF1-mediated translation using polysome profiling of vector- or YTHDF1-overexpressing HCT116 cells with RUVBL1/2 knockout (**Fig. 5A**), YTHDF1 overexpression increased enrichment of mRNA in the monomer assemblies 40S, 60S, and 80S compared with control cells, accompanied by a partial increase in polysomes. The stronger association of YTHDF1 with the 40S–80S monomers implies its involvement primarily in promoting translation initiation. In contrast, knockout of RUVBL1/2 in YTHDF1-overexpressing cells depleted mRNA binding to 40S, 60S and 80S monomers and polysomes, essentially abrogating the effect of YTHDF1 on translation (**Fig. 5A**). Corresponding Western blot of polysome fractions revealed the co-enrichment of RUVBL1/2, YTHDF1 and other components of translational initiation complex (EIF3K, EIF4A) in <40S and 40S fractions (**Fig. 5A**). One way to distinguish elongation from initiation is by detecting formation of stress granules (27, 28), which are specifically activated by inhibition of translation initiation. We thus determined TIA 1 related (TIAR) protein, a marker of stress granules. Compared with controls, YTHDF1 overexpression inhibited TIAR, while RUVBL1/2 knockout in YTHDF1-overexpressing cells significantly increased TIAR, indicating that the loss of RUVBL1/2 preferentially impaired translation initiation in YTHDF1-overexpressing cells (**Fig. 5B**). These results indicate RUVBL1/2 perform essential function in a complex with YTHDF1 to initiate translation.

RUVBL1/2 knockout inhibits YTHDF1-mediated oncogenic translation involved in MAPK signaling

We thus hypothesize that targeting RUVBL1/2 may impair YTHDF1-mediated protein translation. To prove this, we evaluated the overall translational output in colorectal cancer cells by measuring HPG incorporation into nascent proteins. In line with our notion, HPG incorporation was significantly induced by YTHDF1, indicative of increased protein synthesis (**Fig. 5C**). Meanwhile, RUVBL1/2 knockout largely abolished YTHDF1-induced HPG incorporation (**Fig. 5C**). In parallel, we performed puromycin incorporation assay, another marker of protein translation. Consistent with HPG assay, puromycin uptake into proteins was induced by YTHDF1 overexpression, an effect reversed by knockout of RUVBL1/2 (**Fig. 5D**; Supplementary Fig. S5C). These highlight the critical role of RUVBL1/2 in support of YTHDF1-mediated protein translation.

To decipher the pathways in which translation were suppressed by RUVBL1/2 knockout in YTHDF1-OE cells, we performed ribosome-sequencing, followed by GSEA-KEGG analysis of downregulated genes. Compared with YTHDF1-OE alone, cells with

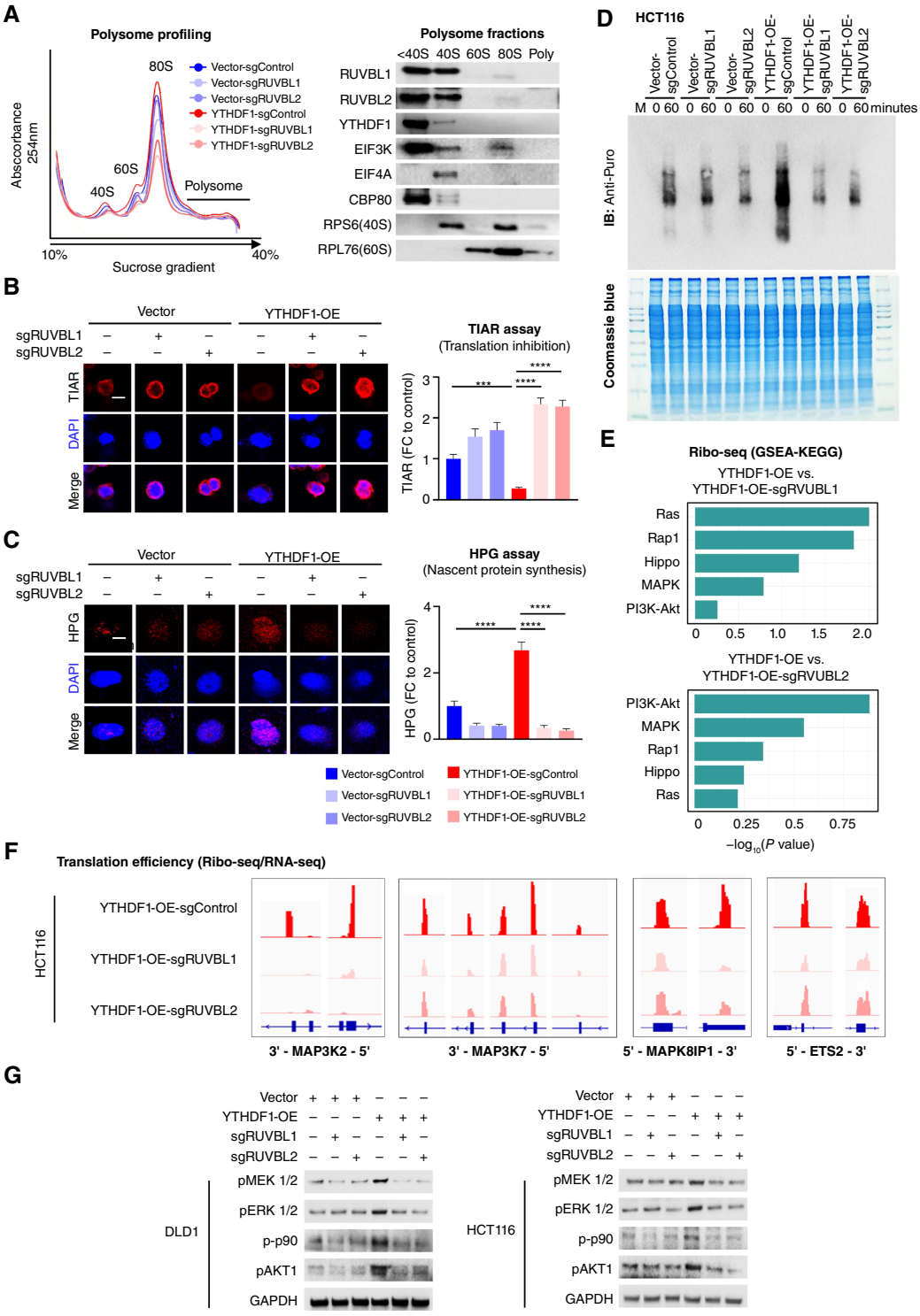

Figure 5.

RUVBL1/2 knockout abrogated YTHDF1-induced translation initiation and oncogenic signaling. **A,** Left, polysome profiling of HCT116 cells with overexpression of YTHDF1 with or without knockout of RUVBL1/2. Right, Western blot of ribosomal fractions (<40S, 40S, 60S, 80S and polysomes). **B,** Stress granules (SG) were determined by immunofluorescence staining of TIA1-related protein (TIAR). **C,** HPG protein incorporation assay for the detection of nascent protein synthesis by immunofluorescence staining. **D,** Puromycin incorporation assay of protein synthesis. **E,** Ribo-seq of YTHDF1-overexpressing HCT116 cells with or without RUVBL1/2 knockout, following GSEA-KEGG pathway enrichment analysis. **F,** Effect of RUVBL1/2 knockout on the translation efficiency of MAP3K2, MAP3K7, MAPK8IP1, and ETS2 in HCT116 cells with YTHDF1 overexpression. **G,** Western blot of MAPK and PI3K-Akt signaling markers. One-way ANOVA (**B** and **C**). ***, $P < 0.001$; ****, $P < 0.0001$.

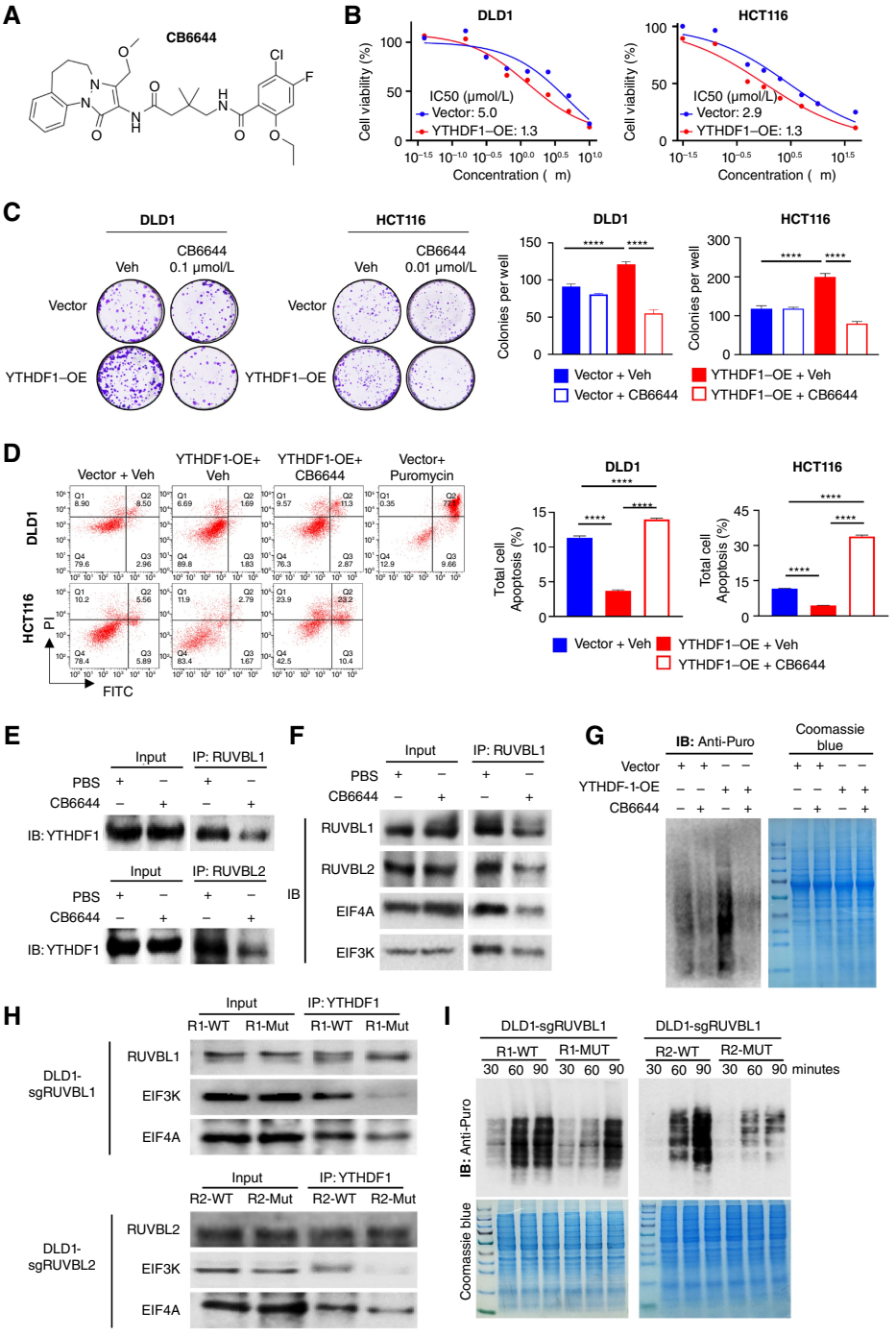

Figure 6.

Pharmacological RUVBL1/2 inhibitor inhibits the growth of YTHDF1-overexpressing colorectal cancer cells. **A,** Structure of a RUVBL1/2 complex inhibitor, CB6644. **B,** Forty-eight hours-IC_{50} values indicated that CB6644 preferentially inhibited the growth of DLD1 and HCT116 cells with YTHDF1 overexpression. **C,** CB6644 preferentially impaired colony formation capacity in YTHDF1-overexpressing DLD1 and HCT116 cells (7–14 days). **D,** CB6644 (0.5 μmol/L for DLD1; 0.1 μmol/L for HCT116, 24 hours) abrogated suppressive effect of YTDHF1 overexpression on apoptosis. Puromycin (0.5 μg/mL, 24 hours) was used as positive control. **E,** Treatment of DLD1 cells with CB6644 (0.5 μmol/L, 36 hours), followed by coimmunoprecipitation to analyze their interactions with YTHDF1. **F,** Interaction between YTHDF1 and EIF3K or EIF4A after treatment with CB6644 in DLD1 cells (0.5 μmol/L, 36 hours). **G,** Effect of CB6644 on protein translation in DLD1 cells, as assessed by puromycin incorporation assay (0.5 μmol/L, 6 hours). **H,** DLD1 cells expressing sgRUVBL1 or sgRUVBL2 were overexpressed with wildtype or ATPase-dead mutant RUVBL1 or RUVBL2, respectively. Coimmunoprecipitation was performed with anti-YTHDF1 to determine its interaction with RUVBL1/2, EIF3K, and EIF4A. **I,** Effect of ATPase-dead mutant RUVBL1 or RUVBL2 on protein translation in DLD1 cells compared with wildtype counterparts. One-way ANOVA (**E** and **F**). ****, $P < 0.0001$.

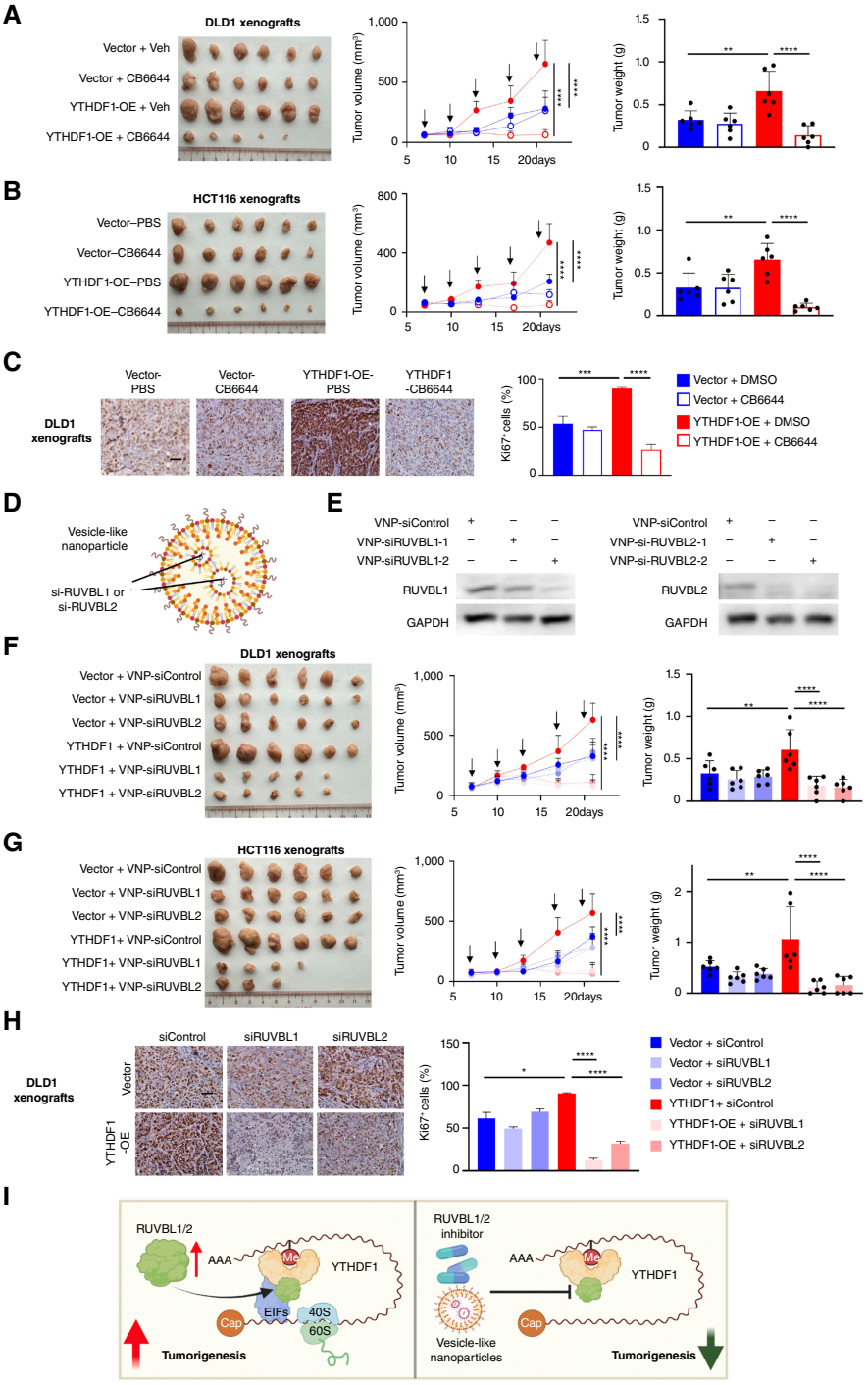

Figure 7.

In vivo efficacy of RUVBL1/2 inhibitors or vesicle-like nanoparticle-encapsulated siRUVBL1/2. **A,** DLD1 vector- or YTHDF1-overexpressing xenografts were treated with CB6644 (25 mg/kg, i.t.; arrows). **B,** HCT116 vector- or YTHDF1-overexpressing xenografts were treated with CB6644 (25 mg/kg, i.t.; arrows). **C,** Ki67 staining of DLD1 xenografts treated with CB6644. **D,** Structure of si-RUVBL1/2 encapsulated by VNPs. **E,** VNP-siRUVBL1/2 knockdown efficiency was confirmed in HCT116 cells *in vitro*. **F,** Effect of VNP-siRUVBL1/2 (2 mg/kg, i.t.; arrows) on DLD1 xenografts with or without YTHDF1 overexpression. **G,** Effect of VNP-siRUVBL1/2 (2 mg/kg, i.t.; arrows) on HCT116 xenografts with or without YTHDF1 overexpression. **H,** Ki67 staining of DLD1 xenografts treated with VNP-siRUVBL1/2. **I,** Schematic diagram showing the mechanism of RUVBL1/2 blockade in YTHDF1-expressing cells. RUVBL1/2 forms a complex with YTHDF1 and associated translation initiation factors, which is essential for YTHDF1-induced protein translation and oncogenic signaling. RUVBL1/2 themselves are targets of YTHDF1, forming a feedforward circuitry that boosts translation in colorectal cancer. RUVBL1/2 inhibition arrested translation by YTHDF1 and abrogated YTHDF1-induced oncogenic signaling and tumorigenesis. *, $P < 0.05$; **, $P < 0.01$; ***, $P < 0.001$; ****, $P < 0.0001$. (**D** and **I,** Created with BioRender.com.)

knockout of RUVBL1 or RUVBL2 showed the downregulation of genes involved in Ras, MAPK, and PI3K-Akt signaling (**Fig. 5E**). In terms of TE (Ribo-seq/RNA-seq), we identified that key genes involved in MAPK signaling were downregulated upon RUVBL1/2 knockout, including MAP3K2 (MEKK2), MAP3K7 (TAK1), MAPK8IP1, and ETS-2, in YTHDF1-overexpressing cells (**Fig. 5F**), but not in the control cells (Supplementary Fig. S6). Concordantly, Western blot demonstrated that RUVBL1/2 knockout abrogated YTHDF1-induced expression of pMEK1/2, pERK1/2, p-p90, and pAKT1 expression (**Fig. 5G**). Together, RUVBL1/2 knockout abolished YTHDF1-mediated oncogenic translation in MAPK signaling, leading to the inactivation of MEK/ERK/p90 and PI3K-Akt signaling cascades in colorectal cancer cells.

RUVBL1/2 inhibitors suppress malignant properties of YTHDF1-overexpressing colorectal cancer cells *in vitro*

In light of our discovery that RUVBL1/2 depletion preferentially suppressed the growth of YTHDF1-overexpressing colorectal cancer cells, we assessed the effect of RUVBL1/2 inhibitor CB6644 (29) *in vitro* (**Fig. 6A**). Western blot showed that high dose (2 μmol/L) CB6644 downregulated RUVBL1/2 proteins (Supplementary Fig. S7A). Although CB6644 did not affect RUVBL1/2 protein stability (Supplementary Fig. S7B), it suppressed the RUVBL1/2 protein translation, as determined by RNC-qPCR (Supplementary Fig. S7C). Next, cell viability determination of 48 hours-IC_{50} values demonstrated that YTHDF1-overexpressing DLD1 and HCT116 cells were more sensitive to the growth inhibitory effect of CB6644, compared with their respective vector control cells (**Fig. 6B**). Colony formation assay also showed that CB6644 preferentially abrogated YTHDF1-induced colony growth in DLD1 and HCT116 cells (**Fig. 6C**). Flow cytometry of apoptosis demonstrated that CB6644 largely reversed the effects of YTHDF1 in suppressing apoptosis (**Fig. 6D**). In short, RUVBL1/2 inhibitor exerts strong inhibitory effect on YTHDF1-induced oncogenic phenotypes.

To ask whether CB6644 functions by blocking YTHDF1-mediated protein translation, we performed RUVBL1/2 pulldown in CB6644-treated cells (**Fig. 6E**), showing that CB6644 reduced YTHDF1 interacting with RUVBL1/2. Coimmunoprecipitation with anti-YTHDF1 further showed that CB6644 inhibited the interaction of YTHDF1 with RUVBL1/2 and translation initiation factors EIF4A and EIF3K (**Fig. 6F**). Consistent with this, CB6644 arrested YTHDF1-driven protein translation (**Fig. 6G**). To further assess if ATPase activity of RUVBL1/2 is critical for YTHDF1-driven translation, we overexpressed wildtype RUVBL1 or ATPase-dead mutant RUVBL1 (E303Q) in DLD1 cells with RUVBL1 knockout, and also overexpressed wildtype RUVBL2 or ATPase-dead mutant RUVBL2 (E266Q) in DLD1 cells with RUVBL2 knockout (**Fig. 6H**). Consistent with our notion, re-expression of mutant RUVBL1/2 abrogated the interplay of YTHDF1 with EIF4A and EIF3K (**Fig. 6H**) and suppressed YTHDF1-mediated protein translation (**Fig. 6I**) as compared with their wildtype counterparts. These data suggest that ATPase activity of RUVBL1/2 is important for the binding of YTHDF1 with components of translation initiation complex and translation activity.

Inhibitors of RUVBL1/2 and vesicle-like nanoparticles-encapsulated siRUVBL1/2 suppressed the growth of YTHDF1-overexpressing colorectal cancer xenografts *in vivo*

Next, we investigated the therapeutic efficacy of CB6644 *in vivo* by treating vector- or YTHDF1-overexpressing DLD1 and HCT116 xenografts with CB6644 (25 mg/kg/day, i.t.) or vehicle (PBS). CB6644 suppressed growth of DLD1-YTHDF1 and HCT116-YTHDF1 xenografts both in terms of tumor volume and weight (both $P < 0.0001$), but had no effect on the respective vector control xenografts (**Fig. 7A** and **B**; Supplementary Fig. S8). In line with its tumor suppressive effect, CB6644 inhibited cell growth ($P < 0.0001$) in DLD1-YTHDF1 xenografts (**Fig. 7C**). Assessment of organ histology (Supplementary Fig. S9A) and serum markers [ALT, AST, blood urea nitrogen or creatinine (CRE); Supplementary Fig. S9B] revealed no abnormalities in the CB6644-treated mice, implying that CB6644 is nontoxic.

In addition to pharmacological inhibitors, recent studies have shown the potential of siRNA nanoparticles in cancer therapy (30). We thus used FDA-approved formulation materials to construct vesicle-like nanoparticles (VNP) to encapsulate and then deliver siRNAs *in vivo* to target RUVBL1/2 (**Fig. 7D**). To improve *in vivo* stability, all pyrimidine bases (C/U) in both strands of the siRNA were modified with 2′-O-methyl groups. Dispersion of VNPs-encapsulating siRNA was confirmed (siControl: 50.7 nm, siRUVBL1: 58.8 nm and siRUVBL2: 50.7 nm; Supplementary Fig. S10A). Pilot *in vitro* knockdown assay demonstrated VNPs-siRUVBL1/2 (100 nmol/L) effectively reduced RUVBL1/2 protein expression (**Fig. 7E**; Supplementary Fig. S10B) and suppressed cell viability *in vitro* (Supplementary Fig. S10C). We then evaluated efficacy of VNP-siRUVBL1/2 in mice bearing HCT116 (**Fig. 7F**) or DLD1 (**Fig. 7G**) xenografts with or without YTHDF1 overexpression. Mice were randomized and treated with VNPs-siControl, VNPs-siRUVBL1, or VNPs-siRUVBL2 (i.t.). Both VNP-siRUVBL1 or VNPs-siRUVBL2 significantly suppressed growth of DLD1-YTHDF1 and HCT116-YTHDF1 xenografts (both $P < 0.0001$) with tumor regression, but they had no effect on control vector counterparts (**Fig. 7F–G**; Supplementary Fig. S11). Ki67 validated the decreased cell growth of YTHDF1-overexpressing DLD1 xenografts treated with VNP-siRUVBL1 or VNP-siRUVBL2 (both $P < 0.0001$; **Fig. 7H**). Therefore, targeting of RUVBL1/2 preferentially suppressed the growth of YTHDF1-overexpressing colorectal cancer xenografts in mice.

Discussion

YTHDF1 functions as an oncogenic m^6A reader in colorectal cancer; however, drugs targeting m^6A deregulation via YTHDF1 are not available. This study utilized a CRISPR-Cas9 screen to systematically screen druggable genes (>1,000) that preferentially target colorectal cancer with high YTHDF1 expression. We revealed RUVBL1/2 as the top genes preferentially decreased the viability of YTHDF1-high colorectal cancer cells. Mechanistically, we showed YTHDF1 and RUVBL1/2 constitute a positive feedforward loop. YTHDF1 promotes translation of RUVBL1/2, which in turn participates in the YTHDF1-initiation complex driving oncogenic translation. Targeting RUVBL1/2 thus blunted YTHDF1-driven oncogenic signaling, leading to tumor suppression in multiple models.

Based on CRISPR-Cas9 screening, RUVBL1/2 are the top gene preferentially depleted in YTHDF1-overexpressing colorectal cancer cells, while being simultaneously enriched in those with YTHDF1 knockdown, suggesting preferential effect of RUVBL1/2 in the presence of high YTHDF1. We further demonstrated that RUVBL1/2 knockout inhibited growth of YTHDF1-expressing colorectal cancer cells in culture by promoting apoptosis and arresting G_1-S cell cycle phase progression. These results were validated in primary colorectal cancer organoids.

Although RUVBL1/2 knockout suppressed the growth of subcutaneous xenografts in control colorectal cancer cells, it had a proportionately greater inhibitory effect on YTDFH1-high counterparts. RUVBL1/2 overexpression have been reported in a variety of cancers and are potential drug targets (31). However, the determinant of the cellular sensitivity to RUVBL1/2 inhibition remains largely unclear. While RUVBL1/2 blockade inhibits the proliferation of multiple cancer cells (29), here we identified YTHDF1 as a factor contributing to increased sensitivity to RUVBL1/2 knockout. Beyond RUVBL1/2, our CRISPR-Cas9 screens also identified THRB as a potential target in YTHDF1-high colorectal cancer cells. However, THRB encodes a thyroid hormone receptor, and it has been reported to function as a tumor suppressor in colorectal cancer (32). We thus focused on evaluating the dependencies of YTHDF1-high colorectal cancer cells on RUVBL1/2 in this study.

We next deciphered the molecular mechanisms of RUVBL1/2 in YTHDF1-high colorectal cancer. Integrated RNA-seq, m^{6}A-seq and Ribo-seq unraveled that YTHDF1 directly binds to m^{6}A-modified RUVBL1/2 mRNA to promote their protein translation. RUVBL1/2 are ring-shaped heterohexamers that exhibit ATPase and DNA helicase activities, and they are highly dependent on one another for stability (33–35). RUVBL1/2 are known to be required for assembly of multiprotein complexes that are associated with tumorigenesis (36–39), principally at the transcriptional level, such as histone acetyltransferase (40), chromatin remodeling (41), and as a cofactor for transcription factors (42). Nevertheless, its potential function(s) in protein translation is unknown. Here, we demonstrated that RUVBL1/2 protein interacts with YTDHF1 in conjunction with translation initiation factors (EIF3K, EIF4A, and EIF1A1), and this complex is closely associated with <40S and 40S ribosomes, key components of translation initiation complex (43), indicating the involvement of RUVBL1/2 in YTHDF1-mediated translation. Consistent with this, RUVBL1/2 knockout or blockade of ATPase activity largely halted YTHDF1-induced translation initiation and global nascent protein synthesis in colorectal cancer cells. YTHDF1-m^{6}A-RUVBL1/2 axis thus promotes translation of RUVBL1/2 as essential components of YTHDF1-associated translation initiation complexes, forming a positive feedforward mechanism to support YTHDF1-mediated oncogenic translation.

The activation of numerous oncogenic pathways has been linked to YTHDF1-mediated translation in colorectal cancer, including WNT/β-catenin, RhoA signaling, as well as MAPK/PI3K signaling (6, 8, 44). We showed that targeting RUVBL1/2 abrogated YTHDF1-induced translation and signaling primarily involving oncogenic MAPK/PI3K signaling, largely consistent with their growth inhibitory effect of RUVBL1/2 in YTHDF1-high colorectal cancer.

YTHDF1 is an emerging therapeutic target in colorectal cancer, and high YTHDF1 expression has been associated with resistance to both chemotherapy (45, 46) and immunotherapy (9). Therefore, targeting YTHDF1-high cells might be a potential approach to improve therapeutic response. To this end, we evaluated two intervention strategies for blocking RUVBL1/2 in YTHDF1-high colorectal cancer. Chemical inhibitor (CB6644) or VNP-siRNA (30) directed silencing RUVBL1/2 both preferentially suppressed the survival of YTHDF1-high colorectal cancer cells *in vitro* and *in vivo*. In agreement with our findings, RUVBL1/2 are emerging targets for cancer, and CB6644 was shown to suppress the growth of Burkitt lymphoma and multiple myeloma cells (29), cancers with high YTHDF1 expression (47, 48). It will be of interest in future studies to evaluate whether RUVBL1/2 inhibitors might potentiate chemotherapy or immunotherapy via depletion of YTHDF1-high colorectal cancer cells. Taken together, our findings suggest RUVBL1/2 as a targetable vulnerability in YTHDF1-high colorectal cancer.

Corroborating our preclinical discoveries, RUVBL1 and RUBVL2 were overexpressed in colon tumors compared with their adjacent normal tissues in independent colorectal cancer cohorts. YTHDF1 protein expression positively correlated with those of RUVBL1/2, suggesting YTHDF1 promotes RUVBL1/2 in humans. Furthermore, RUVBL1 and RUBVL2 proteins were both identified to be independent prognostic factors associated with poor survival in colorectal cancer, in line with their protumorigenic function.

In summary, our systematic survey of the druggable genome identified RUVBL1/2 as druggable targets in YTHDF1-expressing colorectal cancer. YTHDF1-m^{6}A-RUVBL1/2 axis forms a positive feedforward circuitry to promote oncogenic translation, and pharmacological inhibition or nanoparticle-siRNA knockdown of RUVBL1/2 preferentially suppresses growth of YTHDF1-high colorectal cancer growth *in vitro* and *in vivo* (**Fig. 7I**).

Authors' Disclosures

No disclosures were reported.

Authors' Contributions

D. Chen: Data curation, formal analysis, validation, investigation, methodology, writing–original draft. **F. Ji:** Data curation. **Q. Zhou:** Data curation. **H. Cheung:** Data curation. **Y. Pan:** Data curation. **H.C.-H. Lau:** Writing–original draft. **C. Liang:** Data curation. **Z. Yang:** Data curation. **P. Huang:** Data curation. **Q. Wei:** Data curation. **A.H.-K. Cheung:** Formal analysis. **W. Kang:** Data curation. **H. Chen:** Supervision. **J. Yu:** Conceptualization, resources, supervision, funding acquisition, project administration. **C.C. Wong:** Conceptualization, resources, supervision, writing–original draft, writing–review and editing.

Acknowledgments

This project was supported by Research Grants Council (RGC)-Collaborative Research Fund (C4039-19G), RGC-General Research Fund (24100520, 14101917, 14101321), and Health and Medical Research Fund (06170686, 08190706).

Note

Supplementary data for this article are available at Cancer Research Online (http://cancerres.aacrjournals.org/).

Received July 13, 2023; revised November 28, 2023; accepted June 14, 2024; published first June 20, 2024.

References

1. Breekveldt ECH, Lansdorp-Vogelaar I, Toes-Zoutendijk E, Spaander MCW, van Vuuren AJ, van Kemenade FJ, et al. Colorectal cancer incidence, mortality, tumour characteristics, and treatment before and after introduction of the faecal immunochemical testing-based screening programme in The Netherlands: a population-based study. Lancet Gastroenterol Hepatol 2022;7:60–8.
2. Liu Z, Zou H, Dang Q, Xu H, Liu L, Zhang Y, et al. Biological and pharmacological roles of m^{6}A modifications in cancer drug resistance. Mol Cancer 2022;21:220.
3. Wang X, Zhao BS, Roundtree IA, Lu Z, Han D, Ma H, et al. N(6)-methyladenosine modulates messenger RNA translation efficiency. Cell 2015;161:1388–99.

4. Huang H, Weng H, Chen J. m^6A modification in coding and non-coding RNAs: roles and therapeutic implications in cancer. Cancer Cell 2020;37:270–88.
5. Chen H, Gao S, Liu W, Wong CC, Wu J, Wu J, et al. RNA N^6-methyladenosine methyltransferase METTL3 facilitates colorectal cancer by activating the m^6A-GLUT1-mTORC1 axis and is a therapeutic target. Gastroenterology 2021;160:1284–300.e16.
6. Wang S, Gao S, Zeng Y, Zhu L, Mo Y, Wong CC, et al. N6-Methyladenosine reader YTHDF1 promotes ARHGEF2 translation and RhoA signaling in colorectal cancer. Gastroenterology 2022;162:1183–96.
7. Muller S, Glaß M, Singh AK, Haase J, Bley N, Fuchs T, et al. IGF2BP1 promotes SRF-dependent transcription in cancer in a m6A- and miRNA-dependent manner. Nucleic Acids Res 2019;47:375–90.
8. Bai Y, Yang C, Wu R, Huang L, Song S, Li W, et al. YTHDF1 regulates tumorigenicity and cancer stem cell-like activity in human colorectal carcinoma. Front Oncol 2019;9:332.
9. Bao Y, Zhai JN, Chen HR, Wong CC, Liang C, Ding YQ, et al. Targeting m^6A reader YTHDF1 augments antitumour immunity and boosts anti-PD-1 efficacy in colorectal cancer. Gut 2023;72:1497–509.
10. Bai X, Wong CC, Pan Y, Chen H, Liu W, Zhai J, et al. Loss of YTHDF1 in gastric tumors restores sensitivity to antitumor immunity by recruiting mature dendritic cells. J Immunother Cancer 2022;10:e003663.
11. Sanjana NE, Shalem O, Zhang F. Improved vectors and genome-wide libraries for CRISPR screening. Nat Methods 2014;11:783–4.
12. Wan C, Mahara S, Sun C, Doan A, Chua HK, Xu D, et al. Genome-scale CRISPR-Cas9 screen of Wnt/β-catenin signaling identifies therapeutic targets for colorectal cancer. Sci Adv 2021;7:eabf2567.
13. Wang X, Tokheim C, Gu SS, Wang B, Tang Q, Li Y, et al. In vivo CRISPR screens identify the E3 ligase Cop1 as a modulator of macrophage infiltration and cancer immunotherapy target. Cell 2021;184:5357–74.e22.
14. Gao S, Soares F, Wang S, Wong CC, Chen H, Yang Z, et al. CRISPR screens identify cholesterol biosynthesis as a therapeutic target on stemness and drug resistance of colon cancer. Oncogene 2021;40:6601–13.
15. Yang ZJ, Gao SS, Wong CC, Liu WX, Chen HR, Shang HY, et al. TUBB4B is a novel therapeutic target in non-alcoholic fatty liver disease-associated hepatocellular carcinoma. J Pathol 2023;260:71–83.
16. Dauden MI, Lopez-Perrote A, Llorca O. RUVBL1-RUVBL2 AAA-ATPase: a versatile scaffold for multiple complexes and functions. Curr Opin Struct Biol 2021;67:78–85.
17. Li W, Xu H, Xiao T, Cong L, Love MI, Zhang F, et al. MAGeCK enables robust identification of essential genes from genome-scale CRISPR/Cas9 knockout screens. Genome Biol 2014;15:554.
18. Wang YL, DiSalvo M, Gunasekara DB, Dutton J, Proctor A, Lebhar MS, et al. Self-renewing monolayer of primary colonic or rectal epithelial cells. Cell Mol Gastroenterol Hepatol 2017;4:165–182.
19. Tabb DL. The SEQUEST family tree. J Am Soc Mass Spectrom 2015;26:1814–9.
20. Alexa A, Rahnenfuhrer J, Lengauer T. Improved scoring of functional groups from gene expression data by decorrelating GO graph structure. Bioinformatics 2006;22:1600–7.
21. Subramanian A, Tamayo P, Mootha VK, Mukherjee S, Ebert BL, Gillette MA, et al. Gene set enrichment analysis: a knowledge-based approach for interpreting genome-wide expression profiles. Proc Natl Acad Sci U S A 2005;102:15545–50.
22. Langmead B, Salzberg SL. Fast gapped-read alignment with Bowtie 2. Nat Methods 2012;9:357–9.
23. Liao Y, Smyth GK, Shi W. featureCounts: an efficient general purpose program for assigning sequence reads to genomic features. Bioinformatics 2014;30:923–30.
24. Love MI, Huber W, Anders S. Moderated estimation of fold change and dispersion for RNA-seq data with DESeq2. Genome Biol 2014;15:550.
25. Jha S, Dutta A. RVB1/RVB2: running rings around molecular biology. Mol Cell 2009;34:521–33.
26. Shin SH, Lee JS, Zhang JM, Choi S, Boskovic ZV, Zhao R, et al. Synthetic lethality by targeting the RUVBL1/2-TTT complex in mTORC1-hyperactive cancer cells. Sci Adv 2020;6:eaay9131.
27. Liu B, Han Y, Qian SB. Cotranslational response to proteotoxic stress by elongation pausing of ribosomes. Mol Cell 2013;49:453–63.
28. Buchan JR, Parker R. Eukaryotic stress granules: the ins and outs of translation. Mol Cell 2009;36:932–41.
29. Assimon VA, Tang YZ, Vargas JD, Lee GJ, Wu ZY, Lou K, et al. CB-6644 is a selective inhibitor of the RUVBL1/2 complex with anticancer activity. Acs Chem Biol 2019;14:236–44.
30. Zhang Y, Zhang Z, Li S, Zhao L, Li D, Cao Z, et al. A siRNA-assisted assembly strategy to simultaneously suppress "self" and upregulate "eat-me" signals for nanoenabled chemo-immunotherapy. ACS nano 2021;15:16030–42.
31. Armenteros-Monterroso E, Zhao L, Gasparoli L, Brooks T, Pearce K, Mansour MR, et al. The AAA+ATPase RUVBL2 is essential for the oncogenic function of c-MYB in acute myeloid leukemia. Leukemia 2019;33:2817–29.
32. Pourvali K, Shimi G, Ghorbani A, Shakery A, Shirazi FH, Zand H. Selective thyroid hormone receptor beta agonist, GC-1, is capable to reduce growth of colorectal tumor in syngeneic mouse models. J Recept Signal Transduct Res 2022;42(5):495–502.
33. López-Perrote A, Muñoz-Hernández H, Gil D, Llorca O. Conformational transitions regulate the exposure of a DNA-binding domain in the RuvBL1-RuvBL2 complex. Nucleic Acids Res 2012;40:11086–99.
34. Lakomek K, Stoehr G, Tosi A, Schmailzl M, Hopfner KP. Structural basis for dodecameric assembly states and conformational plasticity of the full-length AAA+ ATPases Rvb1 Rvb2. Structure 2015;23:483–95.
35. Yenerall P, Das AK, Wang S, Kollipara RK, Li LS, Villalobos P, et al. RUVBL1/RUVBL2 ATPase activity drives PAQosome maturation, DNA replication and radioresistance in lung cancer. Cell Chem Biol 2020;27:105–21.e14.
36. Munoz DM, Cassiani PJ, Li L, Billy E, Korn JM, Jones MD, et al. CRISPR screens provide a comprehensive assessment of cancer vulnerabilities but generate false-positive hits for highly amplified genomic regions. Cancer Discov 2016;6:900–13.
37. Osaki H, Walf-Vorderwülbecke V, Mangolini M, Zhao L, Horton SJ, Morrone G, et al. The AAA+ ATPase RUVBL2 is a critical mediator of MLL-AF9 oncogenesis. Leukemia 2013;27:1461–8.
38. Rousseau B, Ménard L, Haurie V, Taras D, Blanc JF, Moreau-Gaudry F, et al. Overexpression and role of the ATPase and putative DNA helicase RuvB-like 2 in human hepatocellular carcinoma. Hepatology 2007;46:1108–18.
39. Lauscher JC, Loddenkemper C, Kosel L, Gröne J, Buhr HJ, Huber O. Increased pontin expression in human colorectal cancer tissue. Hum Pathol 2007;38:978–85.
40. Doyon Y, Selleck W, Lane WS, Tan S, Cote J. Structural and functional conservation of the NuA4 histone acetyltransferase complex from yeast to humans. Mol Cell Biol 2004;24:1884–96.
41. Chen L, Cai Y, Jin J, Florens L, Swanson SK, Washburn MP, et al. Subunit organization of the human INO80 chromatin remodeling complex: an evolutionarily conserved core complex catalyzes ATP-dependent nucleosome remodeling. J Biol Chem 2011;286:11283–9.
42. Wood MA, McMahon SB, Cole MD. An ATPase/helicase complex is an essential cofactor for oncogenic transformation by c-Myc. Mol Cell 2000;5:321–30.
43. Aitken CE, Lorsch JR. A mechanistic overview of translation initiation in eukaryotes. Nat Struct Mol Biol 2012;19:568–76.
44. Han B, Yan S, Wei S, Xiang J, Liu K, Chen Z, et al. YTHDF 1-mediated translation amplifies Wnt-driven intestinal stemness. EMBO Rep 2020;21:e49229.
45. Zhang K, Zhang T, Yang Y, Tu W, Huang H, Wang Y, et al. N^6-methyladenosine-mediated LDHA induction potentiates chemoresistance of colorectal cancer cells through metabolic reprogramming. Theranostics 2022;12:4802–17.
46. Sun Y, Dong D, Xia Y, Hao L, Wang W, Zhao C. YTHDF1 promotes breast cancer cell growth, DNA damage repair and chemoresistance. Cell Death Dis 2022;13:230.
47. Xia TL, Li XY, Wang XP, Zhu YJ, Zhang H, Cheng WS, et al. N(6)-methyladenosine-binding protein YTHDF1 suppresses EBV replication and promotes EBV RNA decay. Embo Rep 2021;22:ARTN e50128.
48. Wang J, Zuo Y, Lv C, Zhou M, Wan Y. N6-methyladenosine regulators are potential prognostic biomarkers for multiple myeloma. IUBMB Life 2023;75:137–48.